EFFECTS OF DEFECT VACANCIES ON THE SELF-DIFFUSION IN SILICON AND LITHIUM DIFFUSION IN SILICON CLUSTERS USING CLASSICAL MOLECULAR DYNAMICS

A Thesis

by

SWARN JHA

Submitted to the Office of Graduate and Professional Studies of
Texas A&M University
in partial fulfillment of the requirements for the degree of

MASTER OF SCIENCE

Chair of Committee,	Jorge Seminario
Committee Members,	Perla Balbuena
	Yue Kuo
Head of Department,	M. Nazmul Karim

December 2017

Major Subject: Chemical Engineering

ABSTRACT

With the recent advances in micro-electronics and exponential rise in demand for electronic devices and their miniaturization, it is of utmost importance that self-diffusion phenomena in silicon be well understood. However, self-diffusion of silicon clusters with fraction vacancies is still not well understood as is evident from the fact that the reported values of activation enthalpy of self-diffusion via vacancies range from 3.6 to 4.9 eV, for various experiments carried out in the same temperature range of 650 ^{0}C to 1388 ^{0}C which indicates how imprecise the existing measured values are for the same temperature range. This work overcomes the experimental limitation using molecular dynamics to calculate the self-diffusion coefficients both at room temperature and temperature above the melting point. Silicon clusters of the same spherical geometry and size with varying fraction vacancy have been studied using molecular dynamics and Tersoff potential to estimate phase changes and diffusion coefficients.

At 300 K, the self-diffusion coefficient values vary non-monotonically, i.e. at 7.5 % fraction vacancy the value of self-diffusion coefficient falls to half of its value at 0 % fraction vacancy while it increases by two orders of magnitude at 20 % fraction vacancy. At 2000 K, however, there is only a marginal monotonic increase with gradually varying fraction vacancy. It is found that as fraction vacancy increases, the diffusion coefficient value of lithium in silicon shows non-monotonic behavior for the same number of Li atoms in silicon nanosphere which is an important result in a sense that the behavior of the variation of dopant diffusion with respect to vacancies is directly found in this work. This work thus furthers the understanding on vacancy mediated self-diffusion which can lead to better diffusion control essential to device miniaturization. It also provides information on the dependence of the temperature, energy, pressure and phase changes of the silicon clusters with varying fraction vacancy which can be critical as a guideline for material design and selection for thermoelectric, optoelectronic devices and thermal transducers.

It was also found that charge equilibration, applied to small nanocluster system, gave more precise value of the diffusion coefficient.

ACKNOWLEDGMENTS

I would like to extend my gratitude and a heartfelt thank you to my research advisor Dr. Jorge Seminario for his excellent guidance, support and encouragement throughout the duration of this research work and for being a wonderful advisor. I would also like to thank my research committee faculty members Dr. Perla Balbuena and Dr. Yue Kuo, for their continued guidance and support.

I would like to thank my lab mates Victor, Diego and Narendra for their help during my research. A great thanks to my dear friends Prasanth, Rakesh and all other friends at Texas A&M who made this journey fun and a great experience.

I would like to extend my gratitude to the graduate advisor Dr. Arul Jayaraman, department head Dr. Karim, graduate specialist Mrs. Ashley Stokes and other faculty members of the department of Chemical Engineering who helped me immensely from time to time.

A great thank you to the Texas A&M high performance computing, Artie McFerrin Department of Chemical Engineering, Texas A&M Engineering Experiment Station and Texas A&M University Libraries for the resources used during this research.

CONTRIBUTORS AND FUNDING SOURCES

All work for the thesis was completed by the student, under the advisement of Dr. Jorge Seminario of the Artie McFerrin Department of Chemical Engineering. I would like to acknowledge Dr. Perla Balbuena and Dr. Yue Kuo for their guidance and support during the research work.

There are no outside funding contributions to acknowledge related to the research and compilation of this document.

TABLE OF CONTENTS

LIST OF FIGURES

LIST OF TABLES

CHAPTER I

INTRODUCTION

1.1 Brief overview of molecular dynamics

With faster and more sophisticated computational tools available in the modern world, computer based simulations have become a powerful tool to study complex systems. Molecular dynamics (MD) is one such tool.[1] In molecular dynamics, motions of individual atoms are tracked and followed with time by numerically integrating Newton's equation of motion. The dynamics of the system is defined by classical mechanics where atoms correspond to soft balls and bonds are treated as elastic sticks. On the other hand, the quantum or first principles molecular dynamics considers the quantum nature of chemical bond.[2] Even though quantum MD is better in accuracy than classical MD, it requires way too much computational resources on comparison.[3]

Force is classical MD is given as,

$$\mathbf{F}_i = m_i \frac{d^2\mathbf{r}_i(t)}{dt^2} \tag{1.1}$$

For i-th particle having mass m_i, the position vector is given as $\mathbf{r}_i(t) = (x_i(t), y_i(t), z_i(t))$ where the force at time t is $\mathbf{F}_i$. It is needed to specify the initial positions and corresponding velocities of particles along with instantaneous forces on the particles before solving the above differential equations. Numerical methods are employed to solve the discretized form of the equations to find new positions $\mathbf{r}_i(t+\Delta t)$, in terms of known positions at t, after a time Δt from the initial time t. In molecular dynamics, Verlet algorithm is very common due to its simplicity. It is also relatively more stable. It employs the formula derived from Taylor series expansion of positions $\mathbf{r}_i(t)$ and can be written as

$$\mathbf{r}_i(t+\Delta t) \cong 2\mathbf{r}_i(t) - \mathbf{r}_i(t-\Delta t) + \frac{\mathbf{F}_i(t)}{m_i}\Delta t^2 \tag{1.2}$$

Accurate up to forth power in Δt , the above expression is used to calculate the velocities using leap-frog or Verlet technique and velocities are given as

$$v_i(t) = [r_i(t + \delta t) - r_i(t - \delta t)]/2\delta t \quad (1.3)$$

Depending upon the step size used in integration, the trajectories evolve. It is convenient to use reasonably larger time steps for very long trajectories. Forces on atoms are computed at each step of the integration to find the new position and velocity each time. The typical form of potential energy, U can be given as

$$U = \sum_{i=1}^{N} U(r_i) + \sum_{i=1}^{N} \sum_{\substack{j=1 \\ j \neq i}}^{N} U(r_i r_j) + \sum_{i=1}^{N} \sum_{\substack{j=1 \\ j \neq i}}^{N} \sum_{\substack{k=1 \\ k \neq i,j}}^{N} U(r_i, r_j, r_k) + \cdots \quad (1.4)$$

For accurate modeling of a physical system, the suitability of the potential or the potential energy function used is of very high importance.

One such example of many body potential is the MEAM potential[4-5] which is given as

$$E = \sum_i [F_i(\rho_i) + \frac{1}{2} \sum_{J(\neq i)} \varphi_{ij}(R_{ij})] \quad (1.5)$$

Where, Fi(ρi) is the embedding function, ρi is the background electron density at the site where atom i occupies, and ψ_{ij} (R_{ij}) is the pair interaction between atoms i and j at a distance R_{ij}. The background electron density ρ is composed of several partial electron density terms. Each partial electron density is a function of atomic configuration and atomic electron density.

Table 1.1 Force field parameters

MEAM Library file inputs	MEAM Library file values (Si)	MEAM Library file values (Li)	MEAM Parameter file inputs	MEAM Parameter file values	Tersoff parameters	Tersoff parameter values
elt	Si	Li	lattce(1,2)	112	R	3.0 Å
lat	dia	bcc	Ec(1,2)	56.4992	D	0.2 Å
z	4	8	alpha(1,2)	4.1	m	3
$i_{element}$	14	3	re(1,2)	2.75	γ	1
atwt	28.086	6.94	rho0(2)	3	$\lambda 1$	3.239
alpha	4.87	2.97	rc	10	$\lambda 2$	1.326
b_0	4.8	1.43	delr	0.1	$\lambda 3$	1.326
b_1	4.8	1	C_{max}(1,1,2)	2.81	c	4.838

Table 1.1 Continued

MEAM Library file inputs	MEAM Library file values (Si)	MEAM Library file values (Li)	MEAM Parameter file inputs	MEAM Parameter file values	Tersoff parameters	Tersoff parameter values
b_2	4.8	1.002	$C_{min}(1,1,2)$	0.55	d	2.042
b_3	4.8	1	$C_{max}(1,2,2)$	2.4	cos θ	0
a_{lat}	5.431	3.51	$C_{min}(1,2,2)$	0.45	θ	π/2
e_{sub}	4.63	1.65	$C_{max}(1,2,1)$	2.4	n	22.956
a_{sub}	1	0.87	$C_{min}(1,2,1)$	0.45	β	0.33675
t_0	1	1	$C_{max}(2,2,1)$	2.2	B	95.373
t_1	3.3	0.264	$C_{min}(2,2,1)$	0.35	A	3264.7
t_2	5.105	0.444	nn2(1,2)	1		
t_3	-0.8	-0.2				
rozero	1	1				
ibar	1	0				

Tersoff potential[6-9] used in this work is a very useful multibody potential and is composed of a repulsive part $U_{repulsive}$ and an attractive part $U_{attractive}$. For any three atoms i, j, k the potential is given as

$$U = U_{repulsive}(r_{ij}) + b_{ij}U_{attractive}(r_{ij}) \tag{1.6}$$

Where, r_{ij} is the distance between atoms i and j and b_{ij} is the environmental dependent parameter which weakens the attraction when the coordination number increases. In another form, the Tersoff potential is written as

$$U_{ij} = f_c(r_{ij})[a_{ij}f_R(r_{ij}) + b_{ij}f_A(r_{ij})] \tag{1.7}$$

Where, the repulsive part of the potential is given as

$$f_r(r) = Aexp(-\lambda_1 r) \tag{1.8}$$

and the attractive part is given as

$$f_A(r) = -Bexp(-\lambda_2 r) \tag{1.9}$$

The potential cutoff function is

$$f_c(r) = \begin{cases} 1, & r \le R - D \\ \frac{1}{2} - \frac{1}{2}\sin\frac{\pi}{2}\frac{(r-R)}{D}, & R - D < r < R + D \\ 0, & r \ge R + D \end{cases} \quad (1.10)$$

$$b_{ij} = \left(1 + \beta^n \zeta_{ij}^n\right)^{\frac{-1}{2n}} \quad (1.11)$$

$$\zeta_{ij} = \sum_{k \neq i,j} f_c(r_{ik}) g\left(\theta_{jik}\right) \exp[\lambda_3^3 (r_{ij} - r_{ik})^3] \quad (1.12)$$

$$g(\theta) = 1 + \frac{c^2}{d^2} - \frac{c^2}{d^2 + (h - \cos\theta)^2} \quad (1.13)$$

$$a_{ij} = (1 + \alpha^n \eta_{ij}^n)^{\frac{-1}{2n}} \quad (1.14)$$

$$\eta_{ij} = \sum_{k \neq i,j} f_c(r_{ik}) \exp[\lambda_3^3 \left(r_{ij} - r_{ik}\right)^3] \quad (1.15)$$

To calculate temperature, equipartition theorem of energy is used where we have,

$$\langle \mathrm{E_k} \rangle = \frac{1}{2}\left\langle \sum_{\mathrm{i=1}}^{\mathrm{N}} {|\mathrm{p_i}|^2}/{\mathrm{m_i}} \right\rangle = \frac{3}{2}\mathrm{N k_B T} \quad (1.16)$$

An average energy of ${\mathrm{k_B T}}/{2}$ per degree of freedom, the temperature function may be given as

$$T = \frac{2}{3Nk_B}\langle E_k \rangle \quad (1.17)$$

In cartesian co-ordinates, the general form of equipartition theorem is

$$\left\langle \sum_{i=1}^{N} \boldsymbol{r}_i \cdot \boldsymbol{F}_i^{Tot} \right\rangle = -3Nk_BT \quad (1.18)$$

where, $$\boldsymbol{F}_i^{Tot} = \boldsymbol{F}_i^{Int} + \boldsymbol{F}_i^{Ext}$$

The external force can be represented as,

$$\left\langle \sum_{i=1}^{N} \boldsymbol{r}_i \cdot \boldsymbol{F}_i^{Ext} \right\rangle = -3PV \quad (1.19)$$

$$\left\langle \sum_{i=1}^{N} \boldsymbol{r_i} \cdot \boldsymbol{F_i^{Int}} \right\rangle = 3\langle w \rangle \quad (1.20)$$

Using, $$PV = Nk_BT + \langle w \rangle \quad (1.21)$$

we have, pressure

$$P = \frac{Nk_BT}{V} + \frac{1}{3V}\left\langle \sum_{i=1}^{N} \boldsymbol{r_i} \cdot \boldsymbol{F_i^{Int}} \right\rangle \quad (1.22)$$

1.2 LAMMPS

LAMMPS is the abbreviated form of Large-scale Atomic/Massively Parallel Simulator, a classical molecular dynamics program that models an ensemble of particles in a solid, liquid or gaseous state.[10-13] It uses a variety of force fields and boundary conditions to model atomic, polymeric, biological, metallic, granular and coarse-grained systems. Designed to run on parallel computers, it can also run on a single-processor or desktop. LAMMPS was developed by the US Department of Energy Lab and three companies and is distributed by Sandia National Lab. Molecular dynamics in this work is carried out using LAMMPS.

1.3 VMD

This work makes use of visual molecular dynamics (VMD) software which is a molecular visualization software for displaying and analyzing many molecular systems.[14] Dump files from LAMMPS output have been used to analyze the resulting trajectories of systems and molecules in this work.

CHAPTER II

SILICON NANOCLUSTERS

2.1 Introduction

There have been numerous studies of semiconductor clusters not only because of the interest in their chemical structure but also because of their immense importance in micro and nanoelectronics.[15,16] There have been different approaches to study clusters in the nano range.[17] Silicon clusters with vacancies have been studied because of potential applications ranging from optoelectronics to high energy MEMS devices.[18] Porous silicon structures are potential candidates for anode materials of lithium-ion based batteries. The silicon anode in lithium ion batteries is not a continuous cylindrical structure but exist in spherical lumps. Also, the silicon structure has inherent vacancies which can vary to a certain degree. If silicon based anode systems are to be successfully implemented, then it is extremely important that both the self-diffusion and dopant (Li in this case) diffusion coefficients be known with varying fraction vacancy in the silicon cluster.[19,20] Moreover, with the recent advances in micro-electronics and exponential rise in demand for electronic devices and their miniaturization, it is of utmost importance that self-diffusion phenomena in silicon be well-understood to accurately model dopant diffusion.[21-23] However, self-diffusion of silicon clusters with vacancies is still not well-understood as is evident from the fact that the reported values of activation enthalpy of self-diffusion via vacancies range from 3.6 to 4.9 eV,[24] for various experiments carried out in the same temperature range of 650 ^{0}C to 1388 ^{0}C which indicates how imprecise the existing measured values are for the same temperature range. Also, the experimental limitation imposed by the standard techniques like secondary ion mass spectroscopy (SIMS), where the diffusion length even after reasonable annealing duration of close to 180 days is very small for the depth resolution of SIMS, establishes the further need to calculate self-diffusion coefficient below 850 ^{0}C. Also, there is lack of information on–vacancy contribution to self-diffusion in silicon.

In recent studies, Fang et al.[25] investigated the effect of porosity on thermal conductivity of silicon crystals using non-equilibrium molecular dynamics simulations and found that for nanoporous silica at room temperature, the thermal conductivity was independent of the pore size and depended only on porosity. Huang and Lu[26] explored the relationships between vacancy defects and electrical and thermodynamic properties of silicon and found that both the band gap and heat capacity decreased in silicon crystals with increasing vacancy cluster size. Ural et al.[27] carried out the self-diffusion measurements in the range 800-900 ^{0}C and compared the similarities of native point defects and found that in the temperature range 800-1100 ^{0}C, the interstitial mediated self-diffusion accounted for a fraction of 0.5 to 0.62. It is not well understood as to how the diffusion coefficients vary at temperatures close to room temperature and above the melting point in presence of such fraction vacancies. Presence of vacancies can render the bulk melting point of the silicon nanocluster to change considerably by ~ 100 K and it is intriguing to note the phase changes temperatures in such cases.

Many experiments done have found the diffusion coefficient to be the following Arrhenius behavior,

$$D(T) = D_0 \exp(-A/K_B T) \tag{2.1}$$

where A is the activation enthalpy, K_B is the Boltzmann's constant, D_0 is the pre-factor and is dependent on temperature (T) range of the experiment. Another way of calculating the diffusion coefficient is by using the Einstein's formula according to which

$$D = \frac{1}{6N_t}\sum_1^N < |r_i(t) - r_i(0)|^2 \tag{2.2}$$

Where N is the number of atoms in the system and $r_i(t)$ is the position of i-th atom at time t. $r_i(t)$ are generated using molecular dynamics simulations.

2.2 Problem statement and proposed work

One of the aims is to obtain the self-diffusion coefficient, D of silicon with varying fraction vacancy at room temperature and at a temperature above the melting point. On comparison, the obtained results of self-diffusion coefficients would provide better understanding of the dependence of self-diffusion on the varying fraction vacancy at

different temperatures. This result can be utilized to study the diffusion of dopant atoms like lithium in silicon.

The other goal is to obtain the effects of these fraction vacancies on the heating profile, energy gain rate, pressure and phase changes of the silicon nanospheres. These results would provide useful information about heat capacity, thermal conductivity and phase transition which are crucial in selecting a silicon cluster with certain fraction vacancy for applications in thermoelectrics, thermal transducers and optoelectronic devices.

2.3 Methodology

All of the molecular dynamics (MD) simulations were performed using the Large-Scale Atomic/Molecular Massively Parallel Simulator (LAMMPS) program. A silicon sphere of radius 5 nm is created. This contains a total of 26,133 atoms. For this, first of all a silicon box is formed of appropriate size in LAMMPS. Then the center of this box is located and all atoms which falls within a range of radius 5 nm from this center are selected to create a data file. When a xyz file is created from this data file, a sphere of radius 5 nm can be seen. This data file containing the coordinates of all the atoms in the nanospheres formed the basic structure for deriving the nanospheres with corresponding vacancies of 2.5%, 5%, 7.5%, 10% and 20%. To create a sphere of vacancy 2.5% from the coordinates of the atoms of the nanospheres with 0% vacancy, a total of 654 atoms (which is 2.5% of the total atoms 26,133) are randomly deleted. The new coordinates thus retained are used to create a new data file of a nanosphere with 2.5% vacancy. The same procedure is used to obtain silicon nanospheres of vacancy fraction different to the 0% vacancy fraction to compare and evaluate the effect of such vacancy fractions.

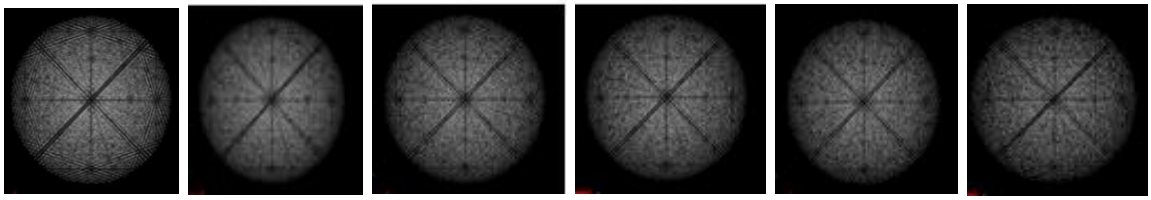

(a) (b) (c) (d) (e) (f)

Figure 2.1. Initial silicon spheres of radius 5 nm with fraction vacancies. Images of a) 0%, 26,133 atoms, b) 2.5%, c) 5%, d) 7.5%, e) 10% and f) 20% vacancy. Si-Si bond length = 1.357 Å

Figure 2.1 shows the snapshots of nanospheres of radius 5 nm with varying vacancy fractions ranging from 0% to 20%. Since the atoms have been randomly deleted, there is no apparent change in appearance of the overall geometry of the sphere for cases with varying vacancy fractions as can be seen from these snapshots.

For the molecular dynamics calculations, the Tersoff potential which is regarded an apt force field for silicon, is used. All calculations are done in metal units, using periodic boundary condition. A time step of 1 fs is used and the ensemble is NVT. The simulation box size is 300 × 300 × 300 $Å^3$ and cutoff distance is 5.2 Å. Now, for a sphere with vacancy, an initial energy minimization is done. This is followed by an equilibration at 5 K for 50,000 timesteps followed by heating to up to 300 K in another 50,000 timesteps. Then again, an equilibration is done at 300 K for 50,000 timesteps. After this, the system is heated to up to about the boiling point temperature of silicon which is about 3538 K in another 50,000 timesteps. This is followed by an equilibration at this temperature for another 50,000 timesteps.

For these different vacancy fraction cases, the plots of temperature vs time, energy vs time and pressure vs time are obtained. Also, radial distribution function plots are obtained for the resulting visualization stages using VMD. The self-diffusion coefficients are calculated at 300 K and at 2000 K respectively using the Einstein's formula.

This is done by calculating one –sixth of the slope of the plot of MSD vs time after equilibration for two nanoseconds.

2.4 Results and discussion

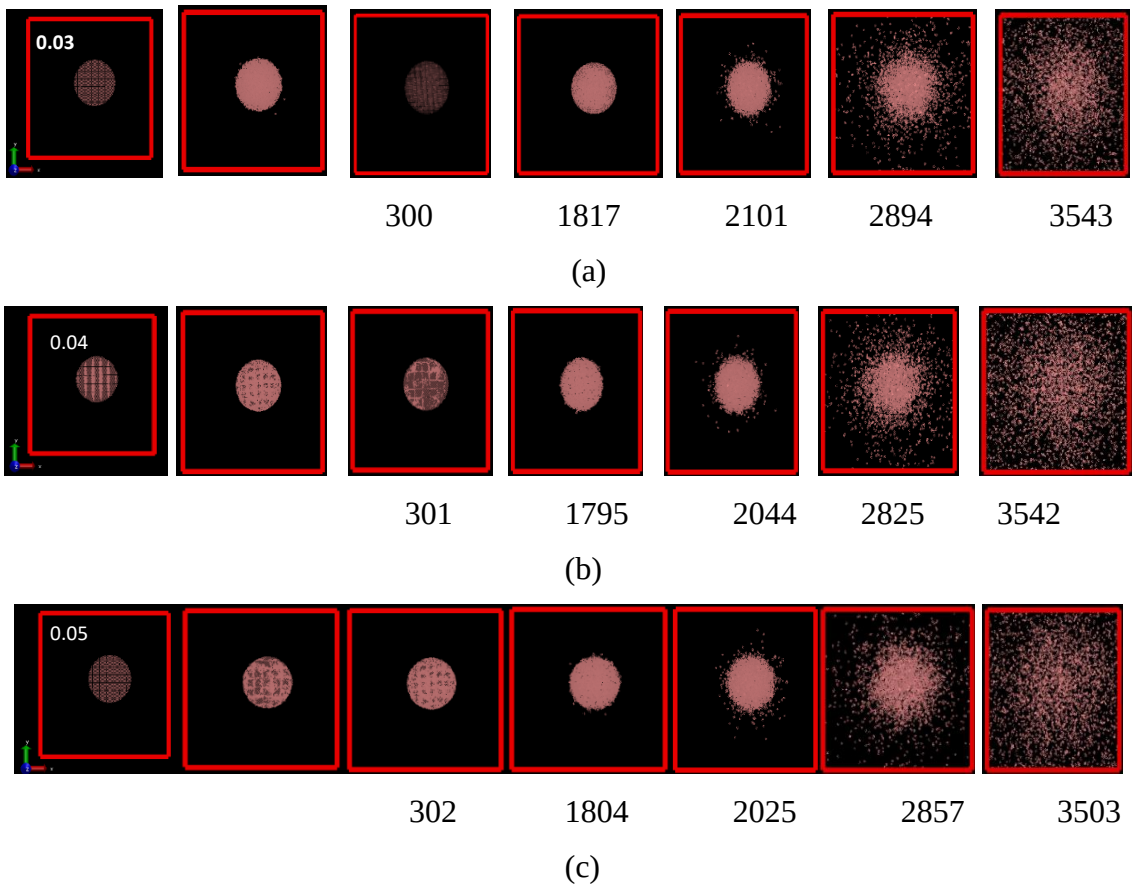

Figure 2.2 Snapshots of the heating of Si nanospheres with fraction vacancies. Images of (a) 0% (b) 2.5% (c) 5% (d) 7.5% (e) 10% (f) 20%. The time (ps) of the snapshot (white top) and temperature (K) (black bottom). Stages of heating: minimization for a-f at 0.03, 0.04, 0.05, 0.05, 0.06, 0.06 ps, respectively; equilibration at 5 K at 50 ps; equilibration at 300 K at 150 ps; intermediate heating stages 300K-3538K at 175, 180, and 190 ps; heating at 3538 K at 200 ps for cases a-f. Radius of the clusters is 5 nm.

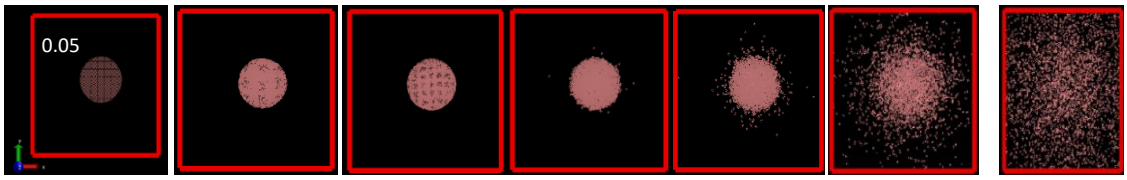

299 1758 2054 2915 3545

(d)

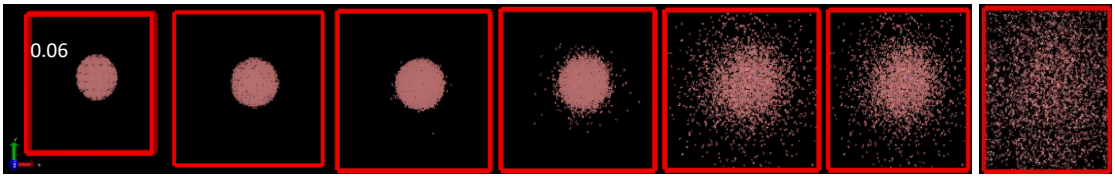

298 1740 2065 2913 3523

(e)

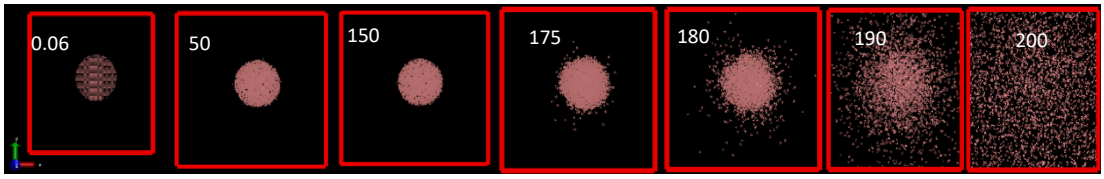

5 5 299 1745 2266 2848 3541

(f)

Figure 2.2 Continued

2.4.1 Phase changes

Figure 2.2 shows visualization stages of silicon sphere of different fraction vacancy at different simulation times with the simulation box clearly depicted in red square boundary. The relative sizes of the silicon spheres can be seen and compared at different times. For any fraction vacancy case, it can be observed from Figure 2.2 that as the simulation time increases from left to right, the silicon sphere gets more diffused in space with rise in temperature. The nanosphere roughly maintains its structure at around 300 K. On being heated from 300 K to 3538 K, the nanosphere gradually loses its shape. Atoms begin to emerge out of the nanosphere above 1600 K, indicating the onset of melting, as the nanosphere reaches the melting point of silicon which is about 1683.15 K. With further

rise in temperature, the nanosphere loses its shape progressively as more and more atoms emerge out of the nanosphere which depicts the progression of melting. However, this progression of structural disorder varies both in time and magnitude for cases with varying fraction vacancy. Here a trend can be observed i.e. nanosphere with higher fraction vacancy apparently has a comparatively more diffused state at the same simulation time. For instance, at 180 ps, the corresponding image of the nanosphere in case e shows more dispersion than that of the nanosphere in case d. However, this is not true when we compare the images of case e and case f for the same 180 ps indicating that the trend does not hold true for all the cases. This indicates at a non-linear and not straightforward relationship between the fraction vacancy and the phase change behavior, as could be inferred from the structural integrity, of nanosphere. Finally, at around 3538 K, which is close to the boiling point temperature of silicon, the nanosphere reaches a state of completely dispersed atoms in space indicative of the boiling point phase behavior. The time for minimization is the least for 0% vacancy case (0.03 ps) and greatest for 20% vacancy case (0.06 ps) indicating that more is the vacancy more is the departure from the most stable energy state.

Only one configuration for each % vacancy is reported here. Theoretically, for a total of n silicon atoms and v number of vacancies there can be C_v^n number of configurations which can be tested. That would require a formidably large amount of time and computational resources. So, this work makes use of a more realistic approach of having a reasonable number of samples (6 nanospheres here) and testing one configuration for each sample to compare the results. So, there is a limitation on the statistics of this work.

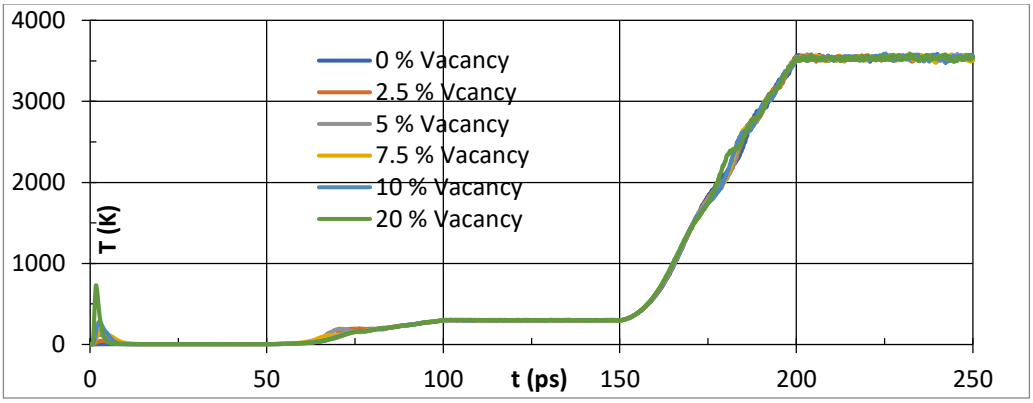

(a)

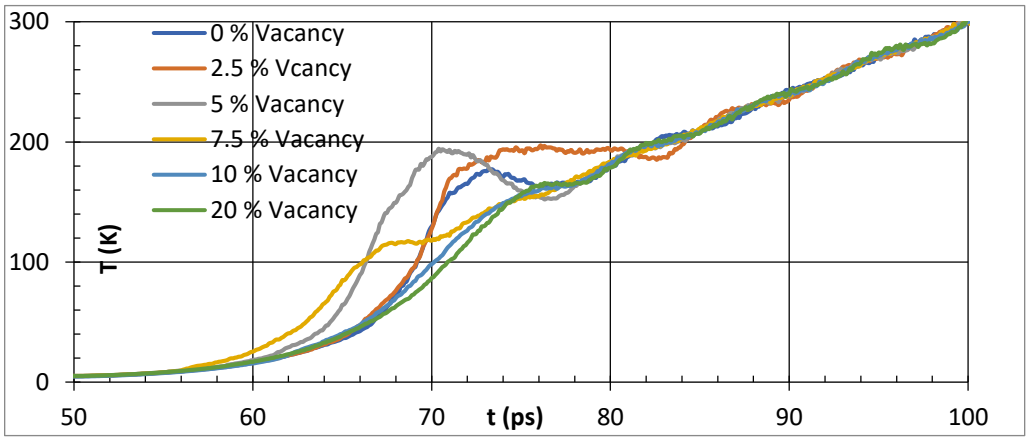

(b)

Figure 2.3. Temperature-time plots for silicon sphere of radius 5 nm with fraction vacancies. Plots for a) Heating and equilibration stages for the entire duration of simulation b) exploded view of heating stage from 5 K-300 K

2.4.2 Temperature changes

Figure 2.3a shows the temperature (T) vs time (t) plot for the silicon nanosphere of radius 5 nm with varying fraction vacancy. For each sample having a fraction vacancy, the simulation proceeds in the order of energy minimization, equilibration at 5 K, heating from 5 K - 300 K, equilibration at 300 K, heating from 300 K- 3538 K and finally equilibration at 3538 K. The rate of heating for these samples, as indicated by the slope of the T-t plot, vary distinctly both between 5 K -300 K and between 300 K – 3538 K. This indicates that

fraction vacancy has a role to play in regulating the heat capacity of nanosphere which affects the way a nanosphere gains temperature.

All the nanospheres have been given the same heating conditions. The idea is to understand the variations in heat gain rate for each nanosphere, in spite of there being the same input heating condition. The fact that in the heating zones particularly (first between 50-100 ps and second between 150-200 ps) there appears to be different heat gain tendencies by each nanosphere which vary in fraction vacancy, indicates that fraction vacancy plays a role in regulating the heat gain rate of the material. The point of interest here is the slope of the T-t curves and their comparison. Of course, if the input heating conditions were different, the slopes would have been different. But the comparison of slopes of T-t for the same input heating conditions is of importance here.

During equilibration at 5 K, the temperature vs time plot shows initial peaks for the cases with certain fraction vacancy and no peak for the case with 0 % vacancy which suggests that there is a sharp rise and fall of temperature on account of atomic rearrangements taking place in the nanosphere due to the presence of vacancy.

Figure 2.3b shows the exploded view for the 5 K – 300 K heating phase of the nanospheres. In this figure we observe that below 200 K there are different heating rates for different nanospheres having varying fraction vacancy whereas above 200 K, the heating rates of various nanospheres are almost the same. The curves have a downwardly concave nature for the 0%, 2.5%, 5%, 7.5 % vacancy cases and have a tendency to linearize for 10% and 20% vacancy cases just below 200 K. This indicates at a non-uniform heating profile for vacancies below 10 % and a tendency toward uniform heating as the vacancy fraction increase. It is not due to the lack in equilibration. All the samples have been equilibrated at 5 K (till 50 ps). As can be seen from the E-t (Figure 2.4) plots for all the samples there is no sharp change or any peaks in the E-t plots for any of vacancies till 50 ps and the plots are smooth horizonal lines indicating the attainment of equilibration. It is only in the

heating zone of 50 – 100 ps that we see in the E-t plots a slight dip or non-linear trajectory of the curve. This is another proof that the nanospheres are showing the above T-t behavior not due to lack of equilibration but due to the presence of fraction vacancies which play a part in regulating the heat gain rate.

A closer observation reveals that for the 0%, 2.5%, 5% and 7.5 % vacancy cases, the temperature rise proceeds with a higher rate, as indicated by a greater slope, starting from around 70 ps reaching a maximum around 75 ps. The temperature rise rate falls after this as indicated by a flatter slope. This effect seems to vanish for the cases with higher vacancy fraction. Thus, while we observe that higher vacancies slow down the rate of heating in general, here we observe a certain temperature below which the role of fraction vacancies become more pronounced (here it appears to be 200 K) and above which it is almost insignificant as to what the system vacancy is in relation to the heating profile of the system. Also, the heating rate of nanospheres do no bear a linear relationship with the fraction vacancy as is substantiated with the fact that below 200 K, the heating rate follows the order 5 %, 2.5 %, 0 %, 7.5 %, 10 % and 20 % from greatest to least. This result could be useful in selecting material with certain fraction vacancy in applications like thermal transducers for temperature below a threshold limit of 200 K.

For the equilibration at 300 K phase, the temperature plots follow a flat trajectory parallel to the time axis. For the 300 K – 3538 K heating phase, the curve for any vacancy fraction case has wave like rise and fall trajectory which indicates at non-uniform heating rate. From 600 K to about 1600 K corresponding to 160 – 172 ps, the slope of the heating curve follows the order 20 %, 10 %, 7.5 %, 5 %, 2.5 % and 0 % from the greatest to the least. Then as the nanospheres approach their melting point temperature i.e. close to 1683 K, the order reverses and the new order becomes 0 %, 2.5 %, 5 %, 7.5 %, 10 % and 20 % from greatest to the least. Thus, the rate of heating reverses the order after the nanospheres attain the melting point temperature. This is a crucial piece of information for applications in thermal transducers right before the melting point of silicon.

To summarize, below the melting point of the silicon clusters, the rate of heating increases as the vacancy fraction increase; however, after the melting point, this order reverses. Also, as the boiling point is approached there is again a shift in order of magnitude of the slopes of each fraction vacancy case. There is clear distinction in heating rates of the nanospheres below and above the melting point and close to the boiling point temperatures which can be attributed to fraction vacancy. This information is useful from the point of view of system selection for a particular heating range based on fraction vacancy consideration.

For the equilibration at 3538 K phase, comparison of temperature-time plot reveals an almost flat trajectory for all the cases.

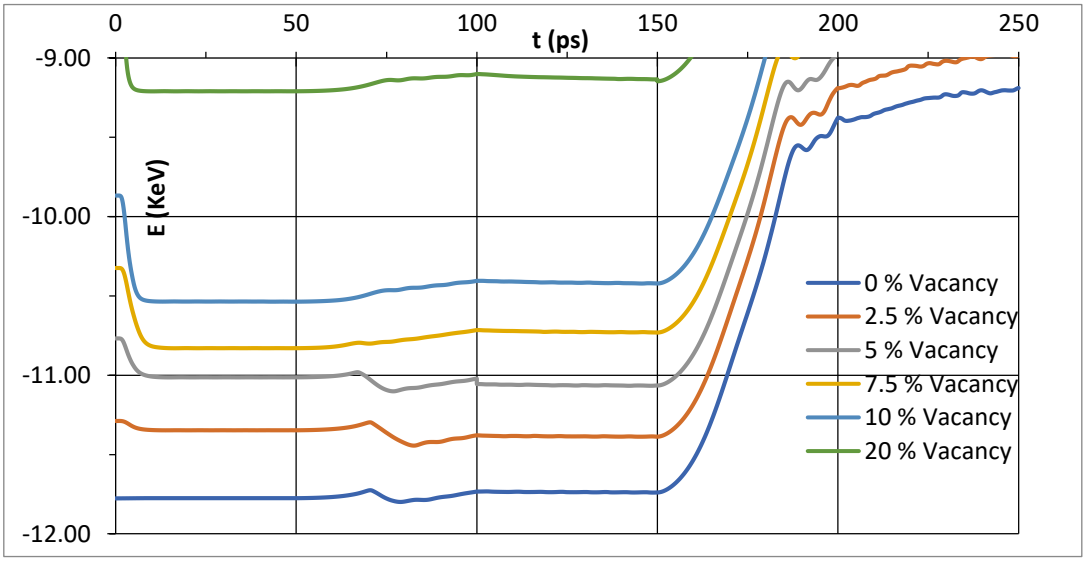

Figure 2.4. Energy-time plots for silicon sphere of radius 5 nm with fraction vacancies

2.4.3 Energy changes

Figure 2.4 shows the energy (E) vs time (t) plots for the silicon nanosphere of radius 5 nm with varying fraction vacancy. It can be seen from the plot that the energy of the 0 %

vacancy case is the least whereas the energy of other fraction vacancy case follows the order 2.5 %, 5 %, 7.5 %, 10 % and 20 % from least to greatest substantiating the fact that more is the fraction vacancy in a nanosphere, more is its energy.

For the equilibration at 5 K, there appears a flat curve for the 0% vacancy case and an initial dip in the curves of cases with certain fraction vacancy. The dip is the largest for the 20% vacancy case. The largest dip in the 20% vacancy case indicates that there is greater degree of rearrangement in this system on account of greater fraction vacancy. However, the total energy of any fraction vacancy case is still larger than that of the 0% vacancy case.

For the 5 K – 300 K heating phase, we observe a dip in the curve at around 70 picoseconds for the 0%, 2.5% and 5% vacancy cases but not for 7.5%, 10% or 20% vacancy cases. This indicates that in this intermediate heating range, the system has a tendency to go to lower energy state at vacancy percent below 7.5% and no tendency to go into lower energy state for a vacancy percent above this value. The total energy of any percent vacancy case is larger than that of 0% vacancy case and follows the order as expected.

For the equilibration at 300 K phase, final energy of the vacancy fraction cases follows the order 0%, 2.5%, 5%, 7.5%, 10% and 20% from the least to the greatest.

For the 300 K-3538 K heating phase, the plot shows that the overall energy is higher for a system with higher fraction vacancy. There could be seen at least two zones where the energy rise rates vary significantly. Considering the 0% vacancy case in particular, starting from about 160 ps the energy rise rate is high and then the rate goes down and follows a lower slope from roughly around 180 ps to up to 200 ps. The transition from first zone to the second happens at around the melting point temperature and the second zone sets in after the melting point is reached. These two zones exist in all the cases of fraction vacancy, but the first zone ends progressively earlier as the fraction vacancy

increase suggesting an earlier phase change for nanosphere with higher fraction vacancy and corresponding lesser rate of energy rise from then on. The energy rise rate falls as the fraction vacancy increase.

For the equilibration at 3538 K phase, the overall energy of the systems follow the order 20%, 10%,7.5%, 5%, 2.5% and 0% from the greatest to the least as expected.

Table 2.1 Energy per atom values for silicon nanospheres with fraction vacancy

% Vacancy	Atoms (no.)	E(KeV)	E/atom
20	20906	-91.458	-0.00437
10	23520	-104.21	-0.00443
7.5	24173	-107.3	-0.00444
5	24826	-110.65	-0.00446
2.5	25480	-113.86	-0.00447
0	26133	-117.4	-0.00449

As per Table 2.1 , it can be seen that the energy per atom (E/atom) value for the least fraction vacancy case i.e 0% vacancy is the least while that of the highest fraction vacancy case i.e 20 % vacancy is the highest. E/atom follows the trend 20 %, 10 %, 7.5 %, 5 %, 2.5 % and 0 % from the greatest to the least.

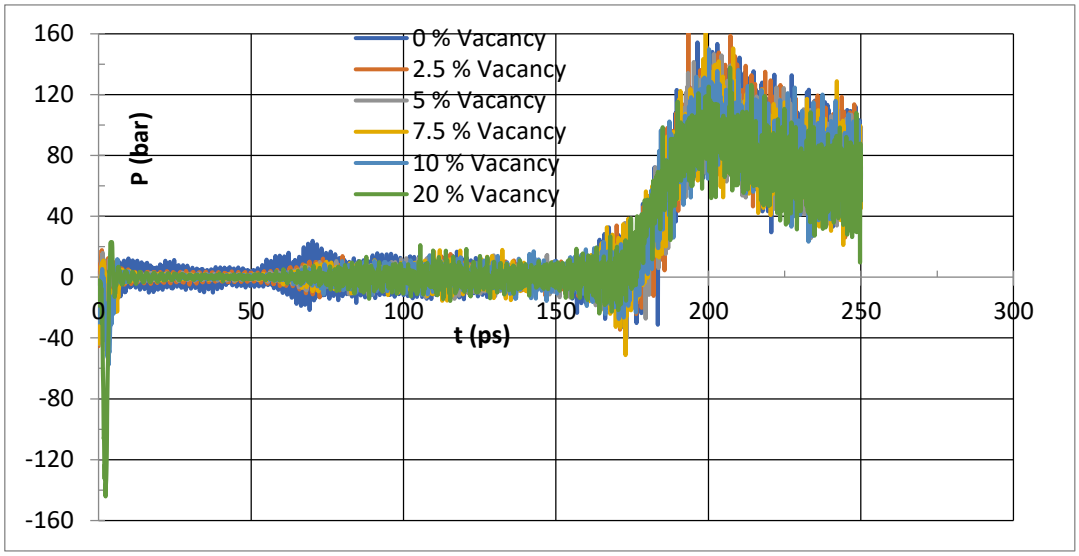

Figure 2.5. Pressure-time plots for silicon sphere of radius 5 nm with fraction vacancies

2.4.4 Pressure changes

Figure 2.5 shows the pressure (P) vs time (t) plots for the silicon nanosphere of radius 5 nm with varying fraction vacancy. For the 5 K – 300 K heating phase, the plot shows that higher the fraction vacancy lesser the fluctuation in pressure of the system and a lesser mean pressure. A left-tapered tail shows that for any fraction vacancy case, as temperature increases, pressure increases and so do the pressure fluctuations. For the 300 K–3538 K heating phase, the plot shows that for any particular case there is steep rise in pressure after the phase change temperature and as the system fraction vacancy increases, this slope rise happens at an earlier time suggesting at earlier achievement of phase temperature. For equilibration at 3538 K, pressure-time plots indicate negative slope of pressure vs time with largest magnitude of slope in the 0% vacancy case which indicates that the pressure of the nanosphere reduces with progressive energy minimization during equilibration and the reduction is maximum for the least fraction vacancy case.

Table 2.2 Temperature, energy and pressure of silicon nanosphere with fraction vacancy at different stages of simulation

Stages after:	t(ps)	T(K)	P(b)	E(KeV)
0% Vacancy				
min	0.03	5	-19.32	-117.76
equil at 5K	50	5.01	1.16	-117.75
heat 5K-300 K	100	299.15	-11.79	-117.33
equil at 300 K	150	300.53	10.4	-117.39
heat300-3538 K	200	3543.75	120.44	-93.76
equil at 3538 K	250	3560.22	64.16	-91.89
2.5 % Vacancy				
min	0.04	5	-45.37	-112.88
equil at 5K	50	5.04	2.65	-113.47
heat 5K-300 K	100	300.61	4.58	-113.79
equil at 300 K	150	301.22	7.2	-113.87
heat300-3538 K	200	3548.99	111.37	-91.9
equil at 3538 K	250	3518.55	71.39	-89.81
5 % Vacancy				
min	0.05	5	-43.66	-103.24
equil at 5K	50	5.13	0.85	-108.23
heat 5K-300 K	100	301.54	-2.22	-107.15
equil at 300 K	150	300.42	1.13	-107.31
heat300-3538 K	200	3540.68	126.01	-87.39
equil at 3538 K	250	3501.79	39.61	-85.28
7.5 % Vacancy				
min	0.05	5	-43.6	-108.14
equil at 5K	50	5.02	-1.59	-110.18
heat 5K-300 K	100	299.21	-2.69	-110.56
equil at 300 K	150	302.3	4.97	-110.65
heat300-3538 K	200	3510.18	100.54	-89.75
equil at 3538 K	250	3555.55	98.72	-87.43
10 % Vacancy				
min	0.06	5	-29.84	-98.67
equil at 5 K	50	4.68	0.011	-105.36
heat 5K-300 K	100	299.71	9.1	-104.04
equil at 300 K	150	298.98	-1.36	-104.21
heat300-3538 K	200	3528.52	105.83	-85.13
equil at 3538 K	250	3555.69	70.84	-82.87

Table 2.2 Continued

Stages after:	t(ps)	T(K)	P(b)	E(KeV)
20 % Vacancy				
min	0.06	5	-14.06	-79.78
min	0.06	5	-14.06	-79.78
heat 5K-300 K	100	298.71	-3.09	-91.14
equil at 300 K	150	296.52	4.28	-91.46
heat300-3538 K	200	3534.7	84.3	-75.99
equil at 3538 K	250	3538.1	80.33	-73.85
equil at 3538 K	250	3555.69	70.84	-82.87

The values for temperature, pressure and energy for the silicon sphere of radius 5 nm and vacancy fraction 0%, 2.5%, 5%, 7.5%, 10% and 20% have been tabulated in Table 2.2. A comparison of the final temperature achieved after the heating stage 5K- 300 K as seen in Table 2.2 for the cases with varying fraction vacancies shows a deviation lying within 2 degrees. However, it is interesting to note the temperature rise rate, as can be seen in Figure 2.3 b, which vary widely across the cases with varying fraction vacancies. This indicates that the vacancy level in a silicon cluster system in this temperature range leads to varying degree of randomness to atomic motions which determines the temperature rise rate. The final temperature reached after the heating stage 300K-3538 K vary within 40 degress, however, as can be seen from Figure 2.3 a, there is apparent considerable variation in temperature rise rate in this heating range which again indicates at the role of vacancy fractions in imparting varying degree of randomness to atomic motions. The final values of energy as seen from Table 2.2 indicates that with increase in vacancy fraction, the energy of the silicon cluster system increases monotonically which is expected due to the greater departure from the crystal structre and hence the resulting rise in instability. The

pressure values in the table for the varying fraction vacancies are non-monotonic in nature and represent the instantaneous values.

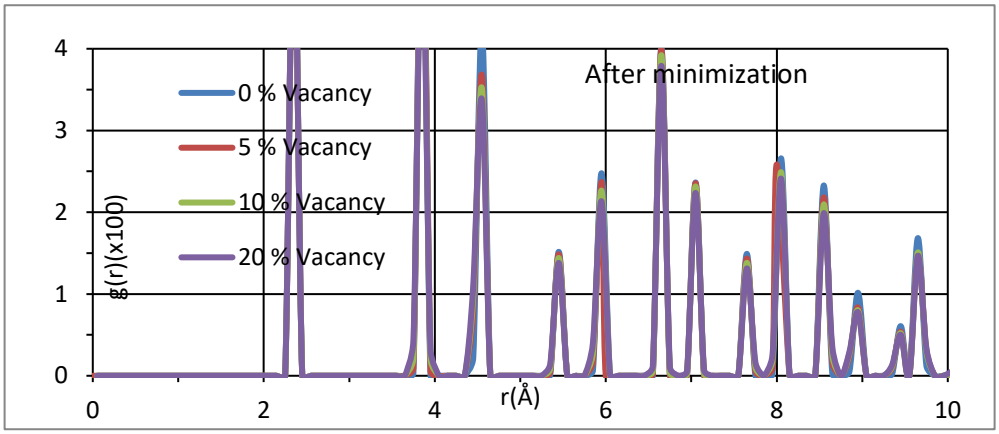

Figure 2.6. RDF plots for silicon sphere of radius 5 nm with varying fraction vacancy at minimization. Step = 0.001 ps, points taken = 1.

2.4.5 Radial distribution function

Figure 2.6 shows the radial distribution function plots obtained after the minimization stage for silicon sphere of radius 5 nm with varying fraction vacancy. It shows several peaks throughout indicating crystal like order in the system. There is no apparent difference in peak positions among the cases with different fraction vacancies.

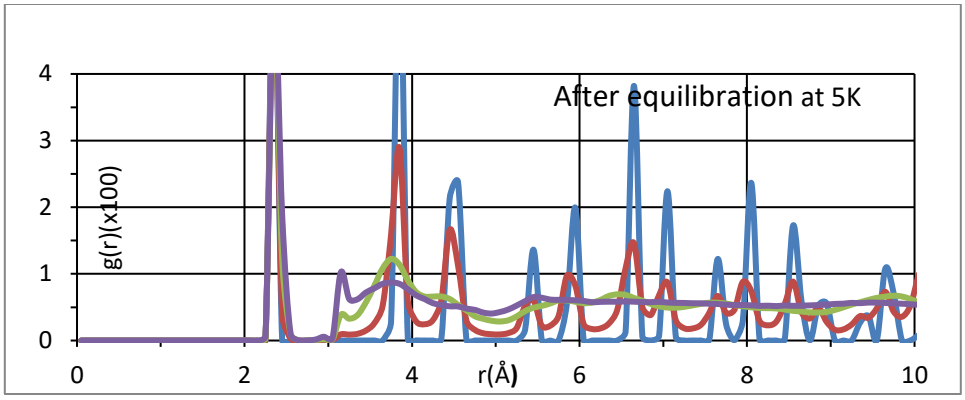

Figure 2.7. RDF plots for silicon sphere of radius 5 nm with varying fraction vacancy after equilibration at 5 K. Step = 0.001 ps, points taken = 1.

Figure 2.7 shows the radial distribution function plots obtained after the equilibration at 5 K for silicon sphere of radius 5 nm with varying fraction vacancy. Comparison of radial distribution function plot shows that as the vacancy fraction increases from 0% to 20%, the peaks shorten in height and the curve has a tendency to flatten out. This indicates that at higher vacancy level the nanosphere is in more diffused state at the same temperature.

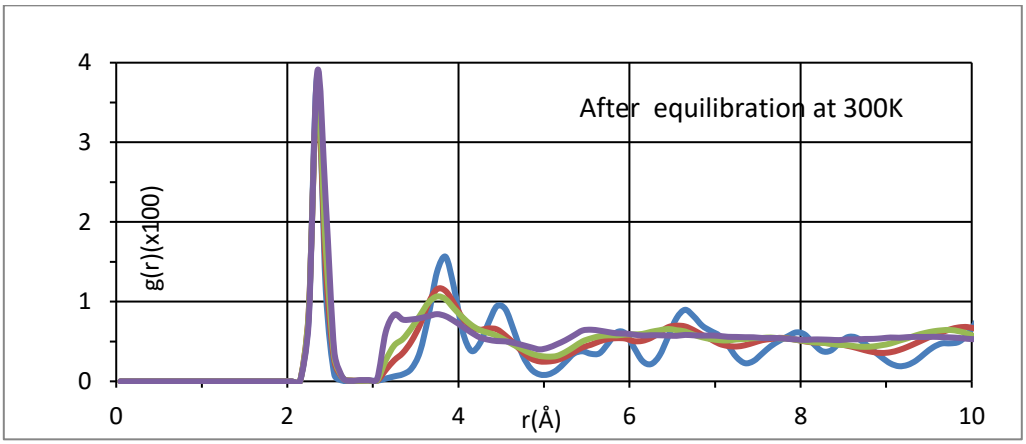

Figure 2.8. RDF plots for silicon sphere of radius 5 nm with varying fraction vacancy after equilibration at 300 K. Step = 0.001 ps, points taken = 1.

Figure 2.8 shows the radial distribution function plots obtained after the equilibration at 300 K for silicon sphere of radius 5 nm with varying fraction vacancy. The radial distribution function plot suggests clearly the relative shortening of peaks for a particular fraction vacancy as we move from 5 K to 300 K which is indicative of vanishing of crystal order in the system. As the vacancy fraction increases from 0% to 20%, the curve tends to flatten suggesting more dispersed phase at 300 K.

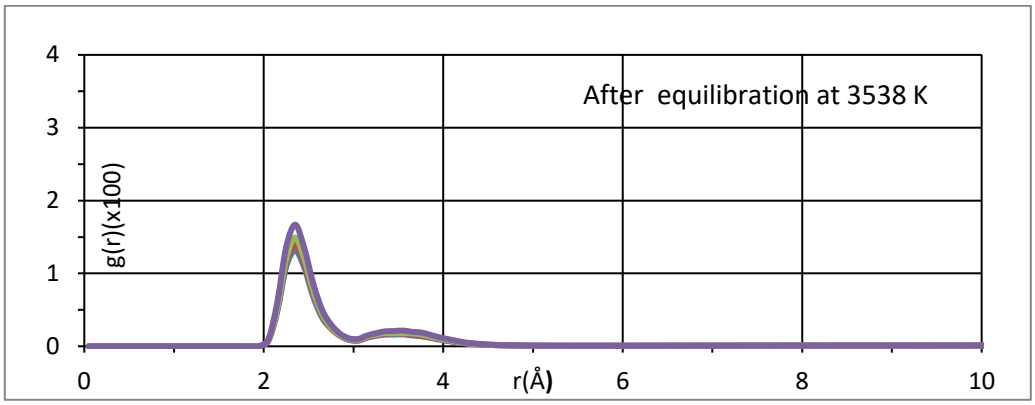

Figure 2.9. RDF plots for silicon sphere of radius 5 nm with varying fraction vacancy after equilibration at 3538 K. Step = 0.001 ps, points taken = 1.

Figure 2.9 shows the radial distribution function plots obtained after the equilibration at 3538 K for silicon sphere of radius 5 nm with varying fraction vacancy. The radial distribution function plot suggests almost similar peak positioning and height for the cases with varying fraction vacancy indicating that at this temperature the nanospheres are more or less at the same dispersed state.

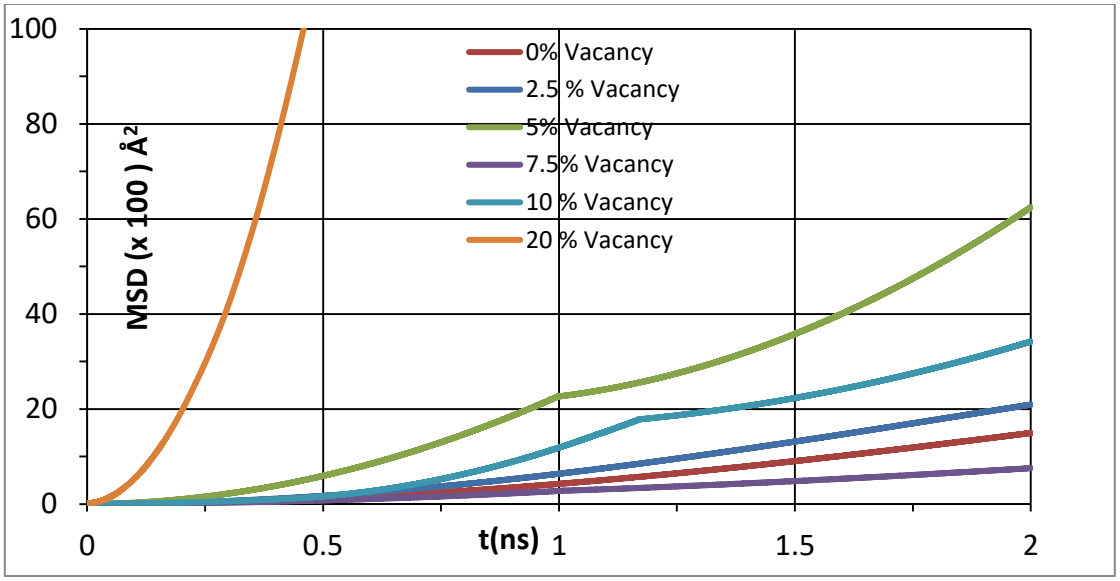

Figure 2.10. MSD-time plot for silicon sphere of radius 5 nm at 300 K and fraction vacancy

2.4.6 Mean square displacement

Figure 2.10 shows the MSD-time plot for silicon sphere of radius 5 nm at 300 K and varying fraction vacancy. It can be seen from the plot that the slope of the various cases with fraction vacancy follow the order 20 %, 5 %, 10 %, 2.5 %, 0 % and 7.5 % from greatest to least. The slope of these individual plots after the samples have been equilibrated for 2 ns are used to calculate the self-diffusion coefficients using Einstein's formula.

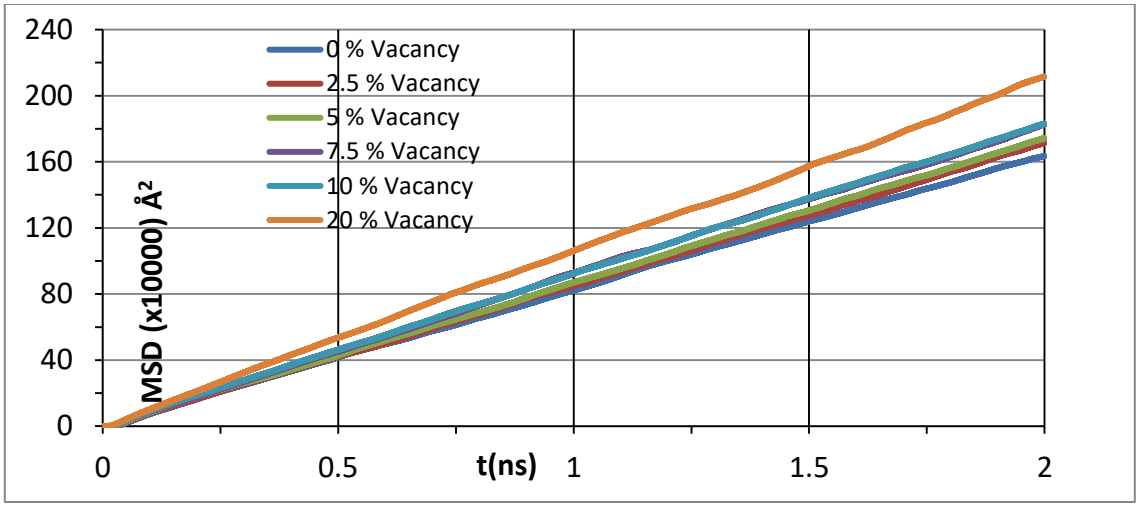

Figure 2.11. MSD-time plot for silicon sphere of radius 5 nm at 2000 K and fraction vacancy

Figure 2.11 shows the MSD-time plot for silicon sphere of radius 5 nm at 2000 K and varying fraction vacancy. It can be seen from the plot that the slope of the various cases with fraction vacancy follow the order 20 %, 10 %, 7.5 %, 5 %, 2.5 % and 0 % from greatest to least. The slope of these individual plots after the samples have been equilibrated for 2 ns are used to calculate the self-diffusion coefficients using Einstein's formula.

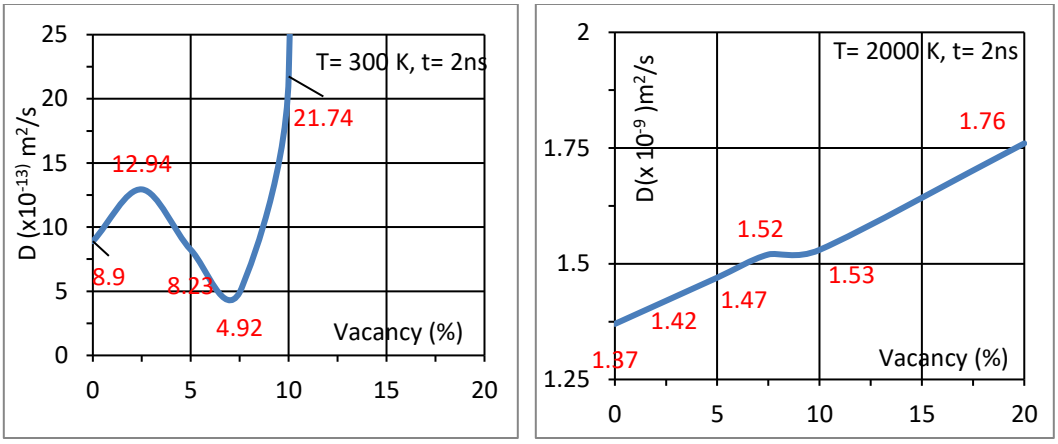

(a) (b)

Figure 2.12. Plots of self-diffusion coefficient (D) at various vacancies for silicon sphere of radius 5 nm (a) at 300 K and time, t = 2 ns (b) at 2000 K and time, t = 2 ns

2.4.7 Self-diffusion coefficient

The self-diffusion coefficient, D values obtained for the systems with varying fraction vacancies are calculated and shown in Figure 2.12 a for 300 K and in Figure 2.12 b for 2000 K. At 300 K, the dependence of D on fraction vacancy is non-linear and non-monotonic. The D value increases as we go to 2.5 % vacancy from 0 % vacancy, then decreases at 5 % and is the least at 7.5 % before increasing steeply at 10 % and 20 % fraction vacancy. The self-diffusion coefficient calculated at 300 K shows that at 5% and 7.5% vacancies, the self-diffusion coefficient is 0.92 times and 0.55 times of the value at 0% vacancy while at 2.5%, 10% and 20% vacancies the value of self-diffusion coefficient of silicon cluster are 1.45 times, 2.44 times, and 86.52 times larger. This result indicates that the value of D is not only dependent on the temperature but also on the fraction vacancy of nanospheres. Also, there is a certain fraction vacancy (7.5 % fraction vacancy in this case) at which the D value is the least and at the same temperature, there can be at least an order of magnitude difference in D values for certain fraction vacancy (20 % fraction vacancy in this case).

At 2000 K, the dependence of D on fraction vacancy is more or less linear and monotonic. D increases with increase in fraction vacancy. D values at 2.5%, 5%, 7.5%, 10% and 20% vacancy increase only marginally and are 1.04 times, 1.07 times, 1.11 times, 1.12 times and 1.28 times respectively at 2000 K. On comparison of D values at 300 K which is close to the room temperature and at 2000 K which is beyond the melting point of silicon, it can be said that in consideration of D calculation, not only the temperature but the fraction vacancy also has a substantial effect. This work thus gives a good understanding of the importance of fraction vacancy in silicon clusters from the point of view of self-diffusion and also useful information about the temperature, energy, pressure and phase changes of the system with varying fraction vacancy. This could be critical for material design and selection of thermoelectrics, optoelectronic devices and thermal transducers to be designed for use in different heating temperature ranges.

The nature of plot 2.12 a is not such due to the lack of equilibration. This is so because when in another trial the same sample was equilibrated for more than 15 ns, using MEAM potential, the self-diffusion calculated was almost the same i.e. 8.7×10^{-13} m^2/s. It may be argued that the statistics is limited here. Theoretically, for a total of n silicon atoms and v number of vacancies there can be C_v^n number of configurations which can be tested for a particular % vacancy. So, there is this limitation in the set of sample size due to time and computational limitation. Also, the number of samples (6 nanospheres here) have been used with due regard to time and computation constraints. Having said so, there is good amount of possibility that the result here is due to the changes in the initial vacancies. This is so because each nanosphere undergoes a change in density even though the density change is marginal. So, the number of vacancies in the final structure is not necessarily the same as in the initial structure. Since, the number of vacancies may have changed in the final structure, so it can be argued that the rate of vacancies formation during the simulation process does not remain the same throughout which affects the mean squared displacement of silicon atoms and hence the self-diffusion coefficient. This rate of

vacancy formation may be somehow related to the extent of fraction vacancy rather than configuration of a nanosphere with certain fraction vacancy.

CHAPTER III

DIFFUSION OF LITHIUM IN SILICON NANOCLUSTERS

3.1 Introduction

In Li-ion batteries, the diffusion of Li determines the reaction velocity of electrode and thus affects the rate performance of the electrode. Thus, Li diffusion kinetics has attracted attentions of many researchers.[28] Reported value of Li diffusion in amorphous silicon are between 10^{-14} to 10^{-18} m^2/s.[29] Many theoretical studies have been done to study the mechanism of Li insertion, to study the diffusion barrier of Li in various silicon structures and geometrical changes[30-31] during lithium insertion and extraction using first principles based density-functional theory.[32-35] Many of the studies focus on energy changes and other static properties of the lithium-ion battery. The dynamics property, such as that of lithium diffusion coefficient in silicon is not very clear at the moment. In this work, we have calculated the diffusion coefficient of lithium in silicon at varying fraction vacancy at room temperature using MEAM potential which can simulate the transition from disordered to ordered Li-Si alloys and predict the material properties of both amorphous and crystalline Li-Si alloys.[36-39]

3.2 Problem statement and proposed work

To obtain diffusion coefficient of lithium in silicon nanosphere with varying fraction vacancy at 300 K is one of the aims of this work. By obtaining the self-diffusion coefficient of silicon and diffusion coefficient of lithium diffusion in silicon at 300 K, we seek to understand better the impact of fraction vacancy on diffusion to address partly the problem of lithium diffusion in silicon for applications like that in the lithium-ion batteries. Understanding of self-diffusion of silicon is the first step as diffusion of any dopant atoms like lithium affects the formation of point defects in silicon and the self-diffusion contribution of those point defects in turn affect the dopant atom diffusion.

3.3 Methodology

Molecular dynamics is carried out using LAMMPS in an NPT ensemble using MEAM potential with cutoff of 5.2 Å and metal units. Periodic boundary condition is used with timestep of 1 fs and 300 × 300 × 300 $Å^3$ simulation box size. To begin with, a silicon nanosphere is created of radius 5 nm which contains a total of 26,133 silicon atoms. Vacancies are induced into this system by randomly deleting atoms from this structure such that resulting nanospheres with fraction vacancies 0%, 5%, and 20% are obtained. To study lithium diffusion in silicon nanoclusters, at first silicon nanosphere with certain fraction vacancy is selected. Then a certain number of lithium atoms is placed at the interstitial sites of the selected silicon nanosphere. This is done by selecting interstitial points randomly in the nanosphere and then placing Li atoms at those points by choosing the coordinates of those selected points for lithium atoms in the data file. Then following steps are carried out in order: minimization at 5 K, equilibration at 5 K, heating 5 K – 300 K, equilibration at 300 K. Temperature vs time, energy vs time and volume versus time plots are then obtained and compared. The self-diffusion coefficients of Li in Si, D is calculated after complete equilibration at 300 K using the Einstein's formula given as

$$D = \frac{1}{6N_t}\sum_1^N < |r_i(t) - r_i(0)|^2$$

3.4 Results and discussion

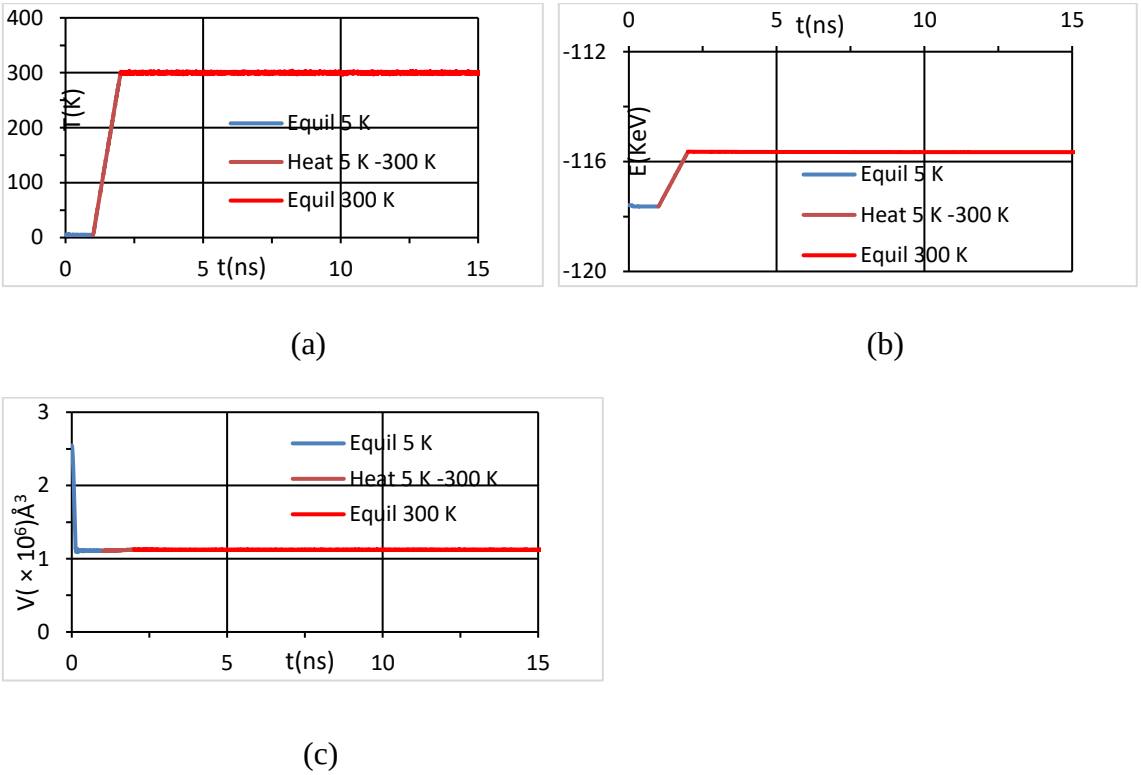

(a) (b)

(c)

Figure 3.1. Plots of (a) Temperature (T) vs Time (t) (b) Energy (E) vs Time (t) (c) Volume (V) vs Time (t) for the nanosphere with 0 % vacancy and 0 lithium atom equilibrated at 5 K (blue), then heated from 5 K – 300 K (orange) then equilibrated at 300 K (red).

3.4.1 0 % Vacancy and 0 Li atom

Figure 3.1 a shows the Temperature (T) vs time (t) plot of the silicon nanosphere with 0 % vacancy and 0 lithium atom. Molecular dynamics simulation is carried out using MEAM potential. The length of time it takes the sample to reach equilibration at 5 K is around 1 ns. After this, it reaches the final temperature of 300 K after about 2.5 ns. The equilibration at 300 K is carried out for a long time and it is only after close to 15 ns that the sample reaches a final equilibrated state suitable for diffusion coefficient calculation. The final equilibrated temperature is about 300 K.

Figure 3.1 b shows the Energy (E) vs time (t) plot for the silicon nanosphere with 0 % vacancy and 0 lithium atom. As can be seen from the plot, the initial equilibrated energy is close to 117 Kev. With gradual heating, as expected, there is rise in energy and the energy after the sample is heated to 300 K is close to 115 KeV. Then the sample is equilibrated till 15 ns to achieve complete equilibration of the sample. Figure 3.1 c shows the Volume (V) vs time (t) plot for the silicon nanosphere with 0 % vacancy and 0 lithium atom. Since the simulation is carried out in an NPT ensemble, hence volume fluctuations are important to note here. The final volume lies between 1- 1.5 million cubic angstrom. For better clarity and analysis, equilibration at 5 K and at 300 K for this nanosphere have been shown below in Figure 3.2 and Figure 3.3 respectively.

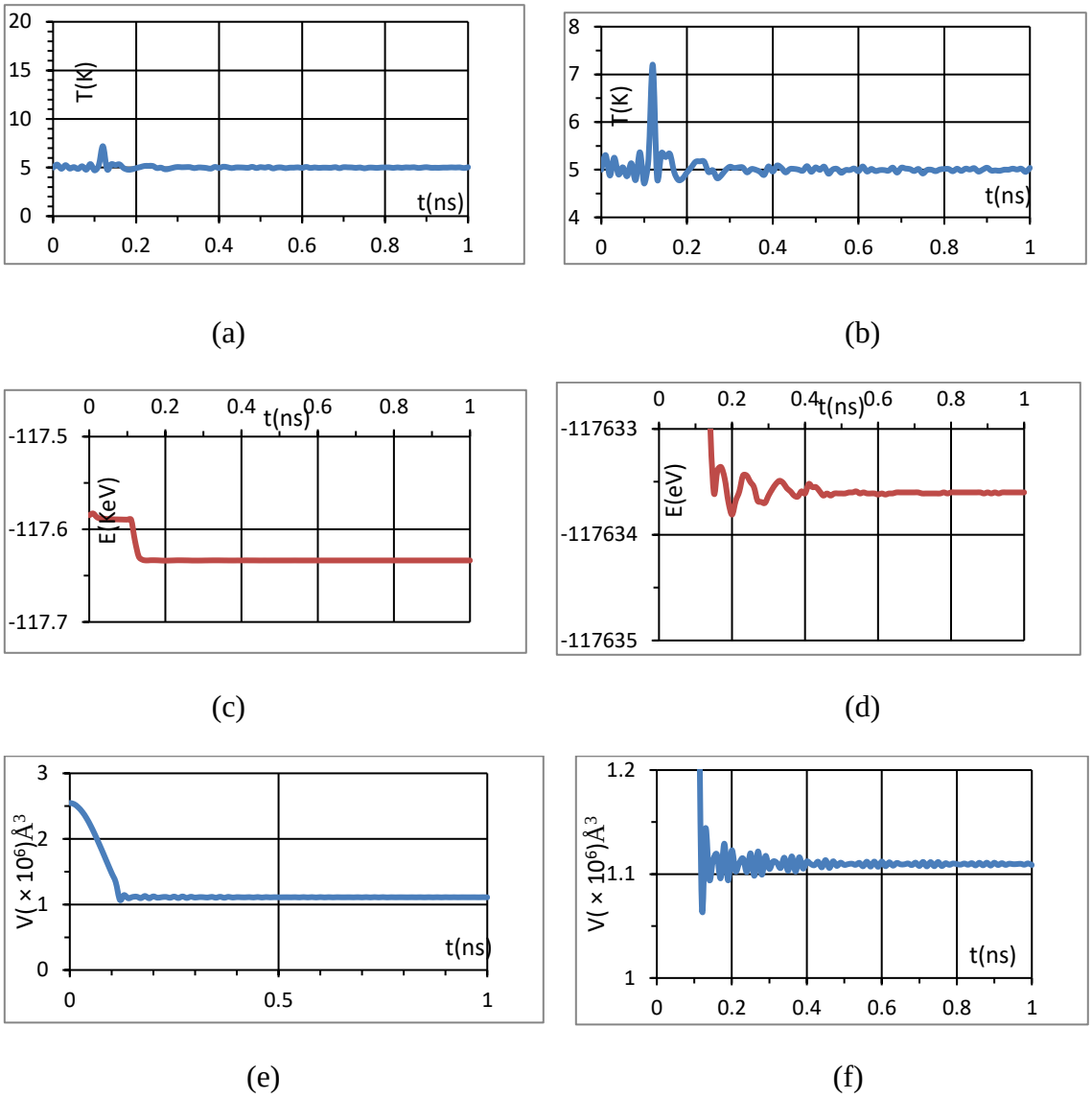

Figure 3.2. Plots of (a) Temperature (T) vs Time (t) (b) exploded view of T vs t (c) Energy (E) vs Time (t) (d) exploded view of E vs t (e) Volume (V) vs time (t) (f) exploded view (V) vs time (t) for the nanosphere with 0 % vacancy and 0 lithium atom at 5 K.

Before the sample is heated to 300 K, it is important that a complete equilibration at 5 K is achieved so that the nanosphere reaches the state of minimum energy corresponding to its actual physical state at 5 K. As can be seen from Figure 3.2 b, there appears an initial peak in T-t plot at around 0.1 ns and the nanosphere's temperature is still fluctuating till

0.4 ns. After this the temperature is more or less constant at 5 K till 1 ns. From Figure 3.2 c it can be seen that there is an initial dip in the E-t plot at around 0.2 ns and after this the energy is more or less constant till 1 ns and lies between -117.6 to -117.7 KeV. From 3.2 d, which is a more zoomed plot of E-t, it can be seen that the energy fluctuations are almost absent after 0.4 ns and the final energy is -11763.5 electron volts. This suggests that a complete equilibration is achieved at 5 K. From Figure 3.2 e it can be seen that the initial volume drops from 2.5 million cubic angstroms to 1 million cubic angstroms in 0.2 ns. From Figure 3.2 f it can be seen that the volume fluctuations are close to nil beyond 0.4 ns and the final volume is around 1.11 million cubic angstroms as the sample reaches complete equilibration at 5 K.

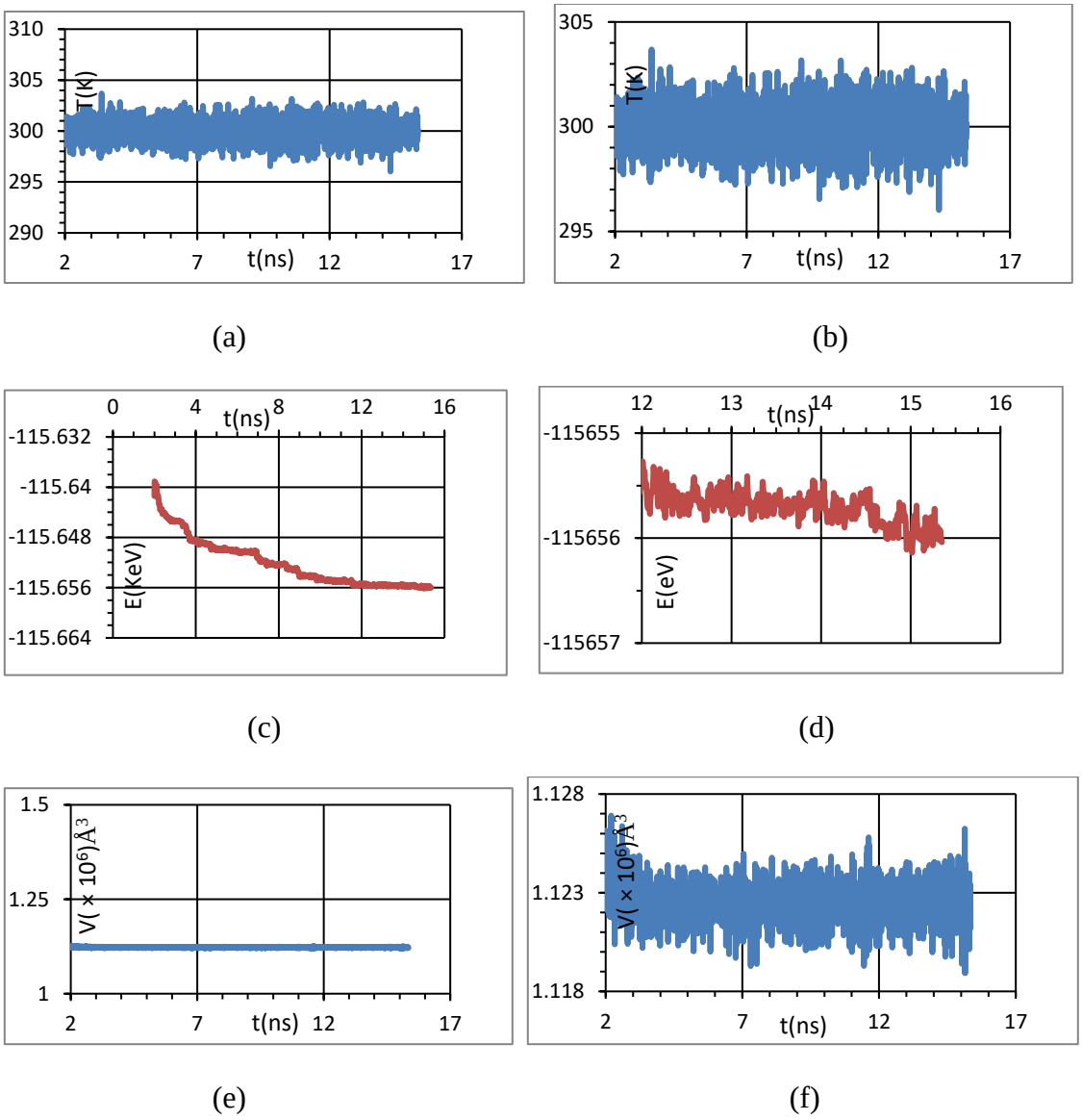

Figure 3.3. Plots of (a) Temperature (T) vs Time (t) (b) exploded view of T vs t (c) Energy (E) vs Time (t) (d) exploded view of E vs t (e) Volume (V) vs time (t) (f) exploded view (V) vs time (t) for the nanosphere with 0 % vacancy and 0 lithium atom at 300 K.

After the sample is heated to 300 K, it is then equilibrated at 300 K. The time of equilibration is such that there is minimal to no change in the energy. As can be seen from Figure 3.3 c, the energy drops from its initial value of -115.64 KeV to -115.656 KeV after about 12 ns. From Figure 3.3 d, it is clear that the final energy stays at around -115656

electron volts which confirms that a complete equilibration is achieved at 300 K. Figure 3.3 a and Figure 3.3 b, show that the temperature of the nanosphere fluctuates around 300 K with the mean value lying at 300 K during the entire course of equilibration step. Figure 3.3 e shows that the volume of the sample lies between 1 to 1.25 million cubic angstroms. Figure 3.3 f shows that the volume fluctuations are around the mean volume of about 1.123 million cubic angstroms.

Having achieved complete equilibration after about 15 ns at 300 K, the diffusion coefficient is now calculated for this sample using the Einstein's formula. The calculated value of the diffusion coefficient is 8.77×10^{-13} m^2/s. Thus, the diffusion coefficient for the case of 0 Li is very much the same as that obtained using the Tersoff potential which was equal to 89×10^{-14} m^2/s. Thus, the values of diffusion coefficients obtained from these two force fields correlates very well.

3.4.2 5 % Vacancy and 100 Li atoms

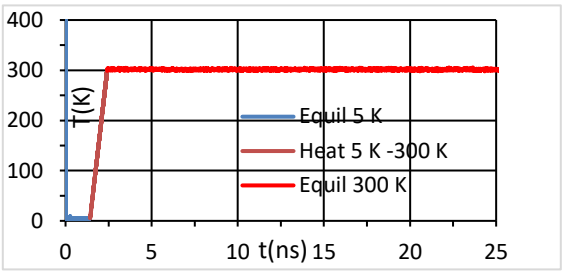

(a)

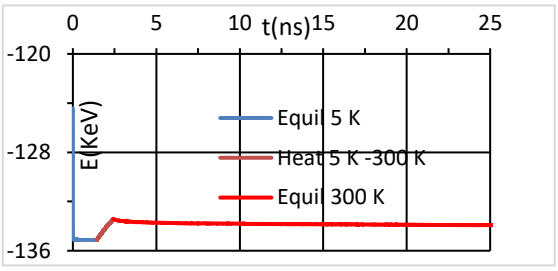

(b)

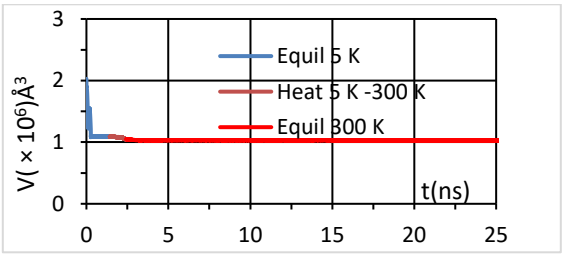

(c)

Figure 3.4. Plots of (a) Temperature (T) vs Time (t) (b) Energy (E) vs Time (t) (c) Volume (V) vs time (t) for the nanosphere with 5 % vacancy and 100 lithium atoms. Sample is equilibrated at 5 K (blue), then heated from 5 K – 300 K (orange) then equilibrated at 300 K (red).

Figure 3.4 a shows the Temperature (T) vs time (t) plot of the silicon nanosphere with 5 % vacancy and 100 lithium atoms. Molecular dynamics simulation is carried out using MEAM potential. The length of time it takes the sample to reach equilibration is around 1.5 ns. After this, it reaches the final temperature of 300 K after about 2.5 ns. The equilibration at 300 K is carried out for a long time and it is only after close to 25 ns that the sample reaches a final equilibrated state suitable for diffusion coefficient calculation. The final equilibrated temperature is about 300 K.

Figure 3.4 b shows the Energy (E) vs time (t) plot for the silicon nanosphere with 5 % vacancy and 100 lithium atoms. As can be seen from the plot, the initial equilibrated energy is close to 135 KeV. With gradual heating, as expected, there is rise in energy and the energy after the sample is heated to 300 K is close to 133 KeV. Then the sample is equilibrated till 25 ns to achieve complete equilibration of the sample.

Figure 3.4 c shows the Volume (V) vs time (t) plot for the silicon nanosphere with 5 % vacancy and 100 lithium atoms. Since the simulation is carried out in an NPT ensemble, hence volume fluctuations are important to note here. The final volume close to 1 million cubic angstrom.

For better clarity and analysis, equilibration at 5 K and at 300 K for this nanosphere have been shown below in Figure 3.5 and Figure 3.6 respectively.

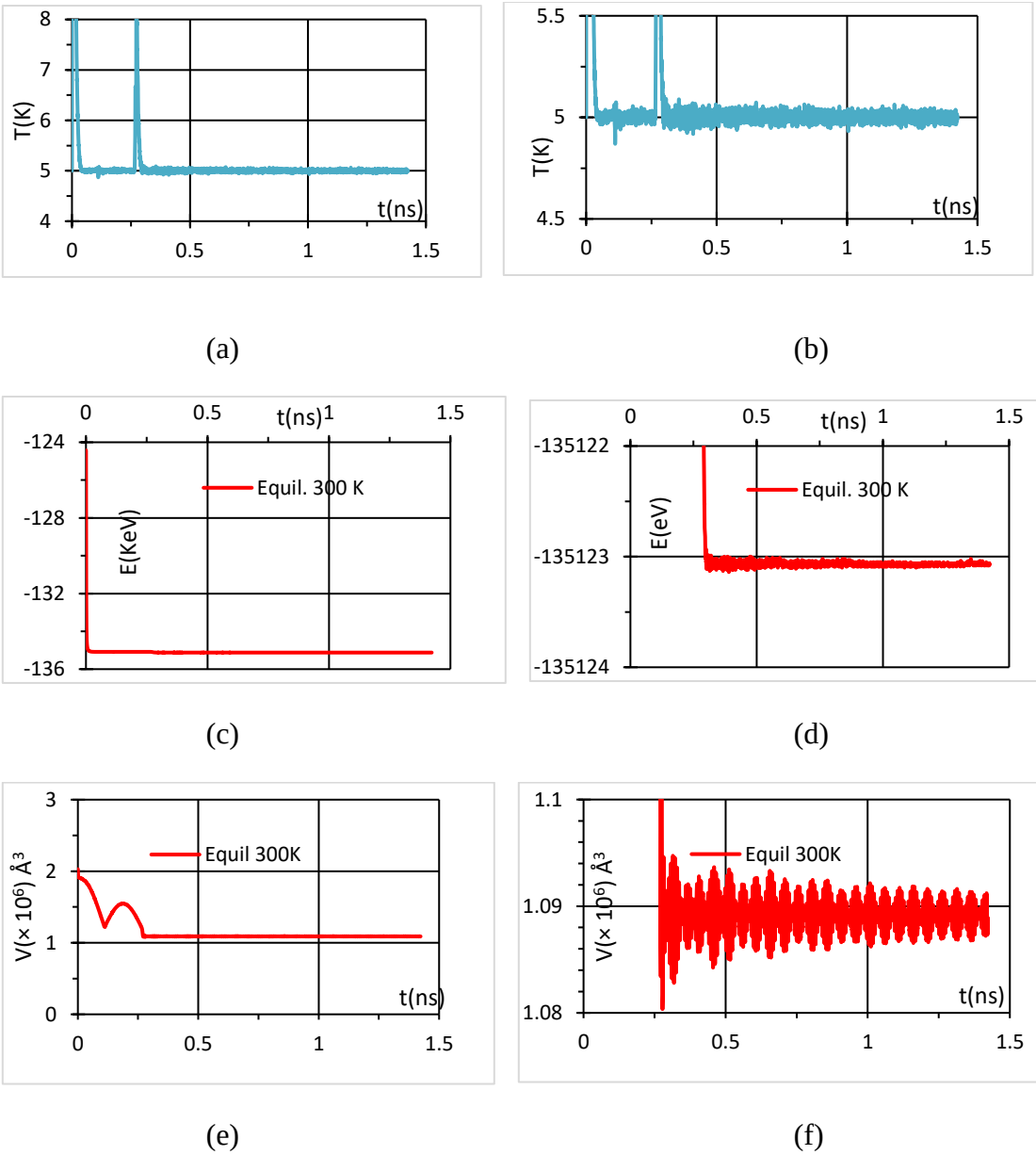

Figure 3.5. Plots of (a) Temperature (T) vs Time (t) (b) exploded view of T vs t (c) Energy (E) vs Time (t) (d) exploded view of E vs t (e) Volume (V) vs time (t) (f) exploded view (V) vs time (t) for the nanosphere with 5 % vacancy and 100 lithium atoms at 5 K.

Before the sample is heated to 300 K, it is important that a complete equilibration at 5 K is achieved so that the nanosphere reaches the state of minimum energy corresponding to its actual physical state at 5 K. As can be seen from Figure 3.5 b, there appears an initial peak

in T-t plot at around 0.25 ns. After this the temperature is more or less constant at 5 K till 1 ns.

From Figure 3.5 c it can be seen that there is an initial dip in the E-t plot at around 0.25 ns and after this the energy is more or less constant till 1 ns and lies close to 135 KeV. From 3.5 d, which is a more zoomed plot of E-t, it can be seen that the energy fluctuations are almost absent after 0.25 ns and the final energy is -135123 electron volts. This suggests that a complete equilibration is achieved at 5 K.

From Figure 3.5 e it can be seen that the initial volume drops from 2 million cubic angstroms to 1 million cubic angstroms in 0.25 ns. From Figure 3.5 f it can be seen that the volume fluctuations beyond 0.25 ns is around 1.09 million cubic angstroms as the sample reaches complete equilibration at 5 K.

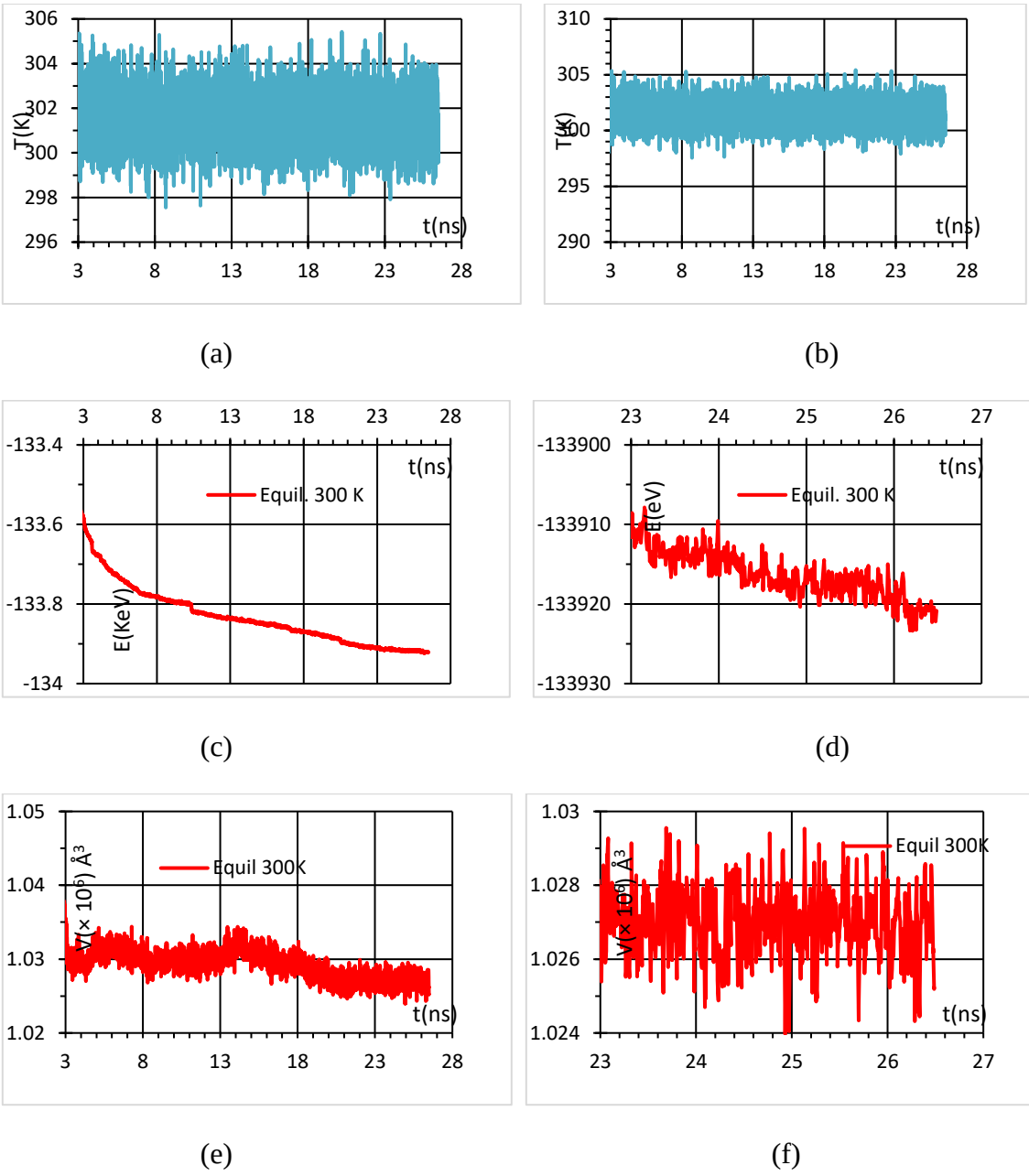

Figure 3.6. Plots of (a) Temperature (T) vs Time (t) (b) exploded view of T vs t (c) Energy (E) vs Time (t) (d) exploded view of E vs t (e) Volume (V) vs time (t) (f) exploded view (V) vs time (t) for the nanosphere with 5 % vacancy and 100 lithium atoms at 300 K.

After the sample is heated to 300 K, it is then equilibrated at 300 K. The time of equilibration is such that there is minimal to no change in the energy. As can be seen from

Figure 3.6 c, the energy drops from its initial value of -133.60 KeV to -133.90 KeV after about 23 ns. From Figure 3.6 d, it is clear that the mean value of the final energy stays at around -133,915 electron volts between 24 to 26 ns which confirms that a complete equilibration is achieved at 300 K. Figure 3.6 a and Figure 3.6 b, show that the temperature of the nanosphere fluctuates around 300 K with the mean value lying at 300 K during the entire course of equilibration step. Figure 3.6 e shows that the volume of the sample lies between 1.02 to 1.04 million cubic angstroms. Figure 3.6 f shows that the volume fluctuations are around the mean volume of about 1.0267 million cubic angstroms after 23 ns when the sample is completely equilibrated at 300 K. Having achieved complete equilibration after about 26 ns at 300 K, the diffusion coefficient is now calculated for this sample using the Einstein's formula. The calculated value of the diffusion coefficient is 0.83×10^{-14} m^2/s.

3.4.3 20 % Vacancy and 100 Li atoms

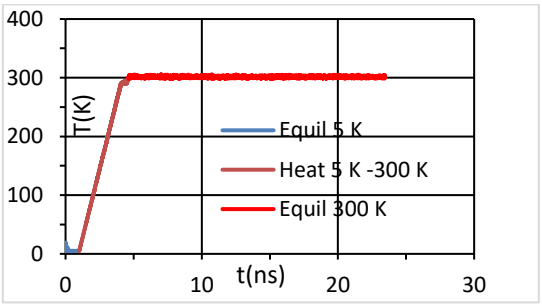

(a)

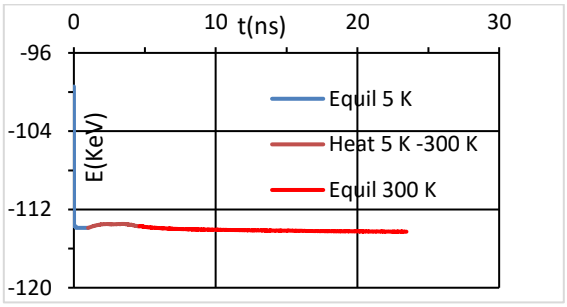

(b)

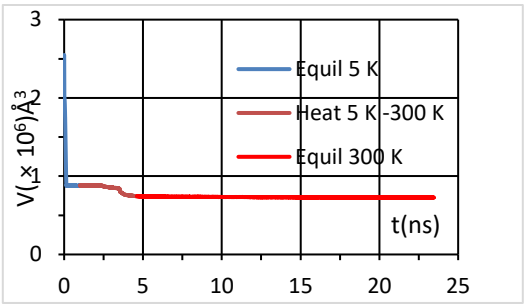

(c)

Figure 3.7. Plots of (a) Temperature (T) vs Time (t) (b) Energy (E) vs Time (t) (c) Volume (V) vs time (t) for the nanosphere with 20 % vacancy and 100 lithium atoms equilibrated at 5 K (blue), then heated from 5 K – 300 K (orange) then equilibrated at 300 K (red).

Figure 3.7 a shows the Temperature (T) vs time (t) plot of the silicon nanosphere with 20 % vacancy and 100 lithium atoms. Molecular dynamics simulation is carried out using MEAM potential. The length of time it takes the sample to reach equilibration at 5 K is around 1 ns. After this, it reaches the final temperature of 300 K after about 5 ns. The equilibration at 300 K is carried out for a long time and it is only after close to 23 ns that the sample reaches a final equilibrated state suitable for diffusion coefficient calculation. The final equilibrated temperature is about 300 K. Figure 3.7 b shows the Energy (E) vs time (t) plot for the silicon nanosphere with 20 % vacancy and 100 lithium atoms. As can be seen from the plot, the initial equilibrated energy is close to 114 KeV. With gradual

heating, as expected, there is rise in energy and the energy after the sample is heated to 300 K is close to 113.5 KeV. Then the sample is equilibrated till about 23 ns to achieve complete equilibration of the sample. Figure 3.7 c shows the Volume (V) vs time (t) plot for the silicon nanosphere with 20 % vacancy and 100 lithium atoms. Since the simulation is carried out in an NPT ensemble, hence volume fluctuations are important to note here. The final volume close to 0.9 million cubic angstroms.

For better clarity and analysis, equilibration at 5 K and at 300 K for this nanosphere have been shown below in Figure 3.8 and Figure 3.9 respectively.

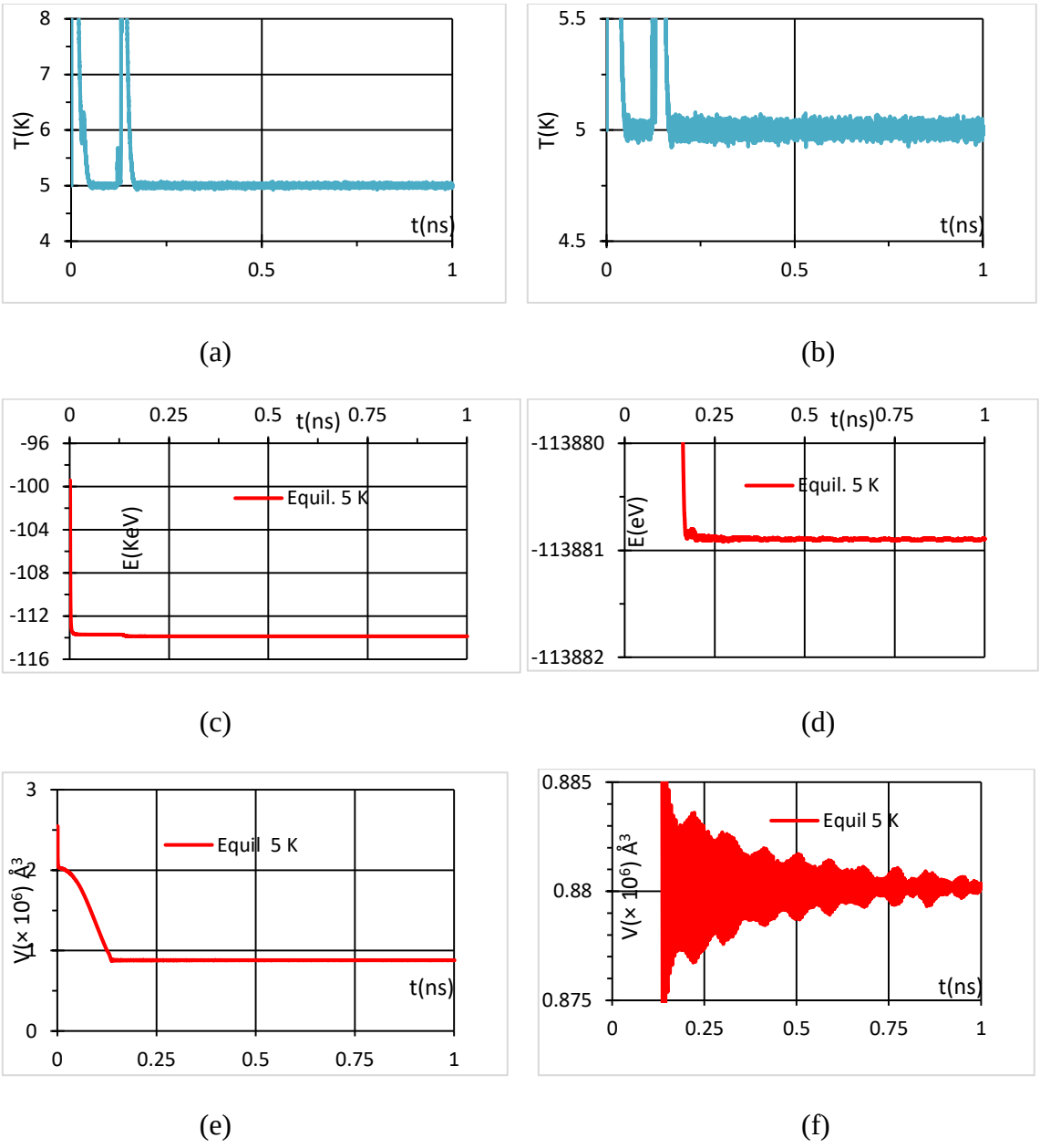

Figure 3.8. Plots of (a) Temperature (T) vs Time (t) (b) exploded view of T vs t (c) Energy (E) vs Time (t) (d) exploded view of E vs t (e) Volume (V) vs time (t) (f) exploded view (V) vs time (t) for the nanosphere with 20 % vacancy and 100 lithium atoms at 5 K.

Before the sample is heated to 300 K, it is important that a complete equilibration at 5 K is achieved so that the nanosphere reaches the state of minimum energy corresponding to its actual physical state at 5 K. As can be seen from Figure 3.8 b, there appears an initial peak

in T-t plot at around 0.125 ns. After this the temperature is more or less constant at 5 K till 1 ns. From Figure 3.8 c it can be seen that there is an initial dip in the E-t plot at around 0.125 ns and after this the energy is more or less constant till 1 ns and lies close to 114 KeV. From 3.8 d, which is a more zoomed plot of E-t, it can be seen that the energy fluctuations are almost absent after 0.125 ns and the final energy is -113,881 electron volts. This suggests that a complete equilibration is achieved at 5 K. From Figure 3.8 e it can be seen that the initial volume drops from 2 million cubic angstroms to close to 0.9 million cubic angstroms in 0.125 ns. From Figure 3.8 f it can be seen that the volume fluctuations beyond 0.125 ns is around 0.88 million cubic angstroms as the sample reaches complete equilibration at 5 K.

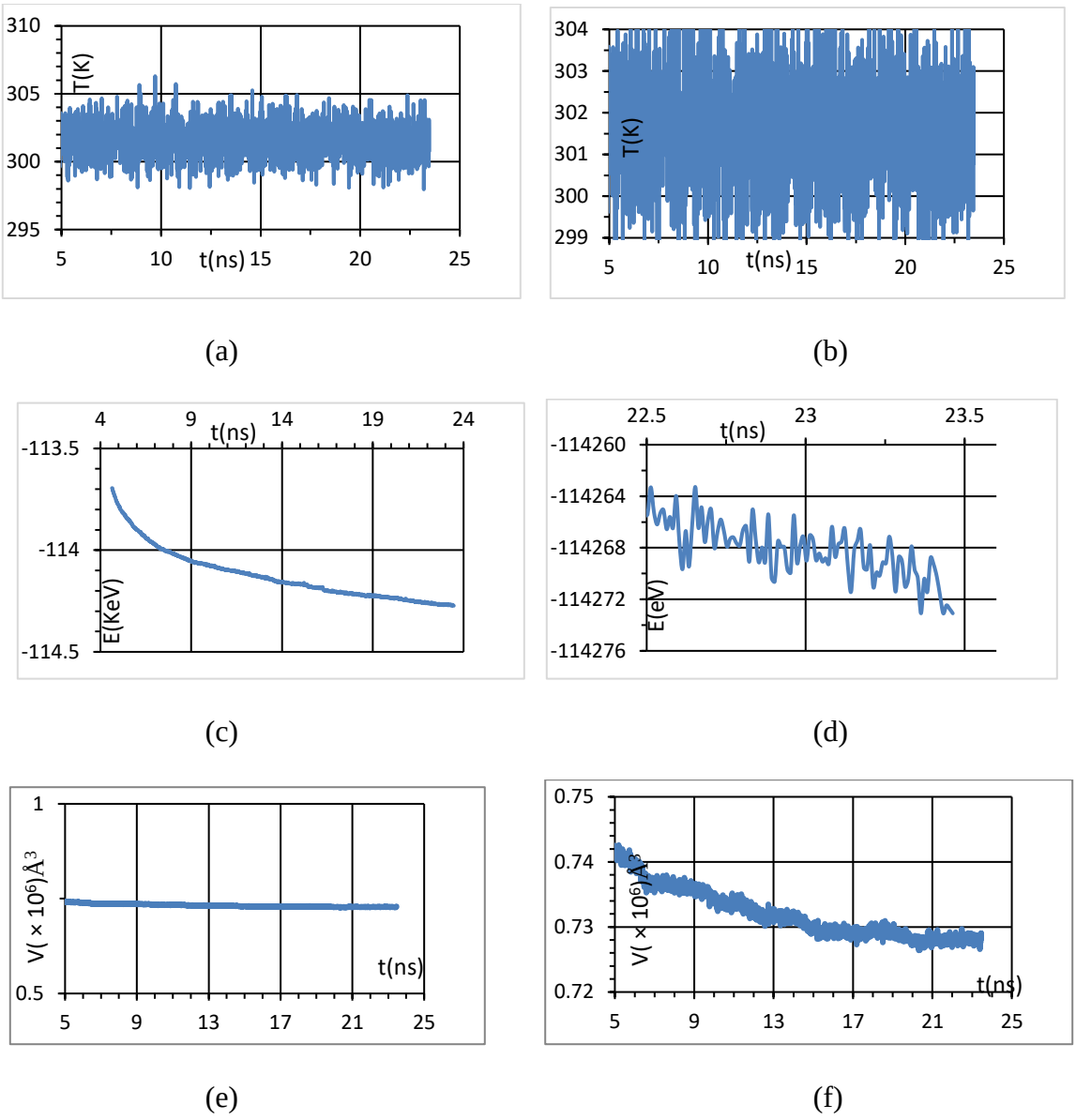

Figure 3.9. Plots of (a) Temperature (T) vs Time (t) (b) exploded view of T vs t (c) Energy (E) vs Time (t) (d) exploded view of E vs t (e) Volume (V) vs time (t) (f) exploded view (V) vs time (t) for the nanosphere with 20 % vacancy and 100 lithium atoms at 300 K.

After the sample is heated to 300 K, it is then equilibrated at 300 K. The time of equilibration is such that there is minimal to no change in the energy. As can be seen from Figure 3.9 c, the energy drops from its initial value of -133.60 KeV to -114.26 KeV after

about 22.5 ns. From Figure 3.9 d, it is clear that the mean value of the final energy stays at around -114,268 electron volts between 22.5 to 23.5 ns which confirms that a complete equilibration is achieved at 300 K.

Figure 3.9 a and Figure 3.9 b, show that the temperature of the nanosphere fluctuates around 300 K with the mean value lying at 300 K during the entire course of equilibration step. Figure 3.9 e shows that the volume of the sample lies between 0.6 to 0.8 million cubic angstroms. Figure 3.9 f shows that the volume fluctuations are around the mean volume of about 0.73 million cubic angstroms after 22.5 ns when the sample is completely equilibrated at 300 K.

Having achieved complete equilibration after about 23 ns at 300 K, the diffusion coefficient is now calculated for this sample using the Einstein's formula. The calculated value of the diffusion coefficient is 1.17×10^{-14} m^2/s.

3.4.4 0 % Vacancy and 100 Li atoms

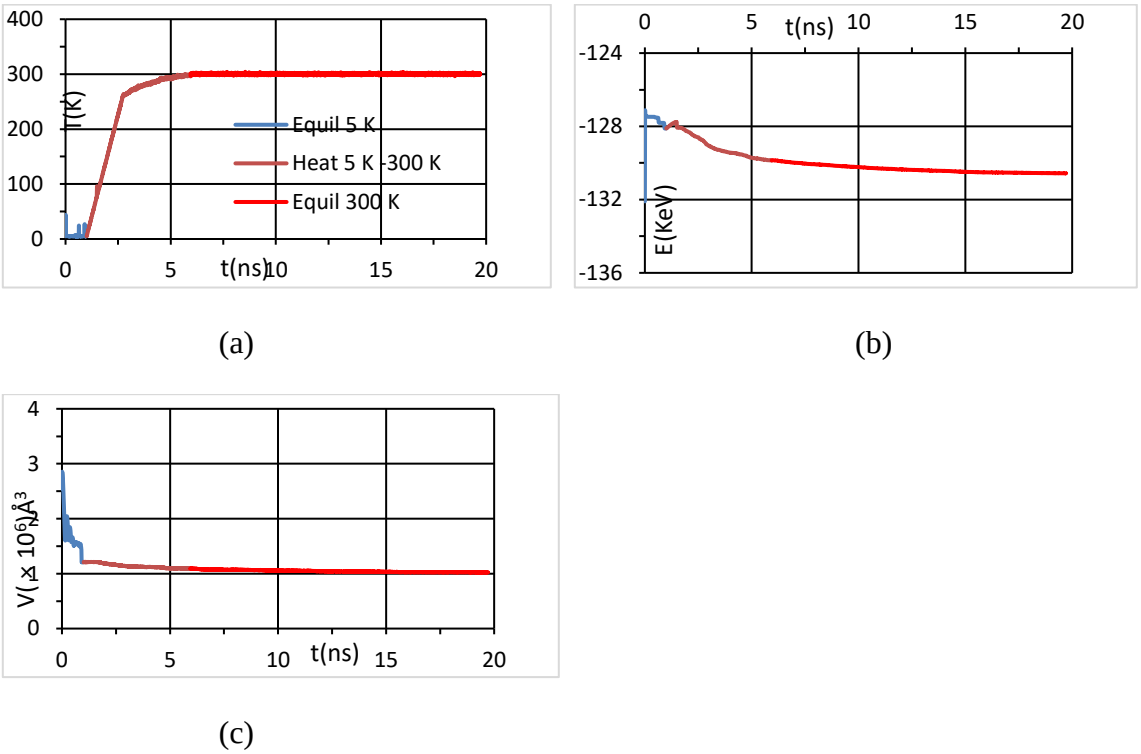

(a) (b)

(c)

Figure 3.10 Plots of a) Temperature (T) vs time (t) b) Energy (E) vs time (t) c) Volume (V) vs time (t) for the nanosphere with 0 % vacancy and 100 lithium atoms equilibrated at 5 K (blue), then heated from 5 K – 300 K (orange) then equilibrated at 300 K (red).

Figure 3.10 a shows the Temperature (T) vs time (t) plot of the silicon nanosphere with 0 % vacancy and 100 lithium atoms. Molecular dynamics simulation is carried out using MEAM potential. The length of time it takes the sample to reach equilibration at 5 K is around 0.6 ns. After this, it reaches the final temperature of 300 K after about 5 ns. The equilibration at 300 K is carried out for a long time and it is only after close to 20 ns that the sample reaches a final equilibrated state suitable for diffusion coefficient calculation. The final equilibrated temperature is about 300 K. Figure 3.10 b shows the Energy (E) vs time (t) plot for the silicon nanosphere with 0 % vacancy and 100 lithium atoms. As can

be seen from the plot, the initial equilibrated energy at 5 K is close to 127.5 KeV. With gradual heating, there is decrease in energy and the energy after the sample is heated to 300 K is close to 130 KeV. Then the sample is equilibrated till about 20 ns to achieve complete equilibration of the sample. Figure 3.10 c shows the Volume (V) vs time (t) plot for the silicon nanosphere with 0 % vacancy and 100 lithium atoms. Since the simulation is carried out in an NPT ensemble, hence volume fluctuations are important to note here. The final volume is close to 1 million cubic angstroms.

For better clarity and analysis, equilibration at 5 K and at 300 K for this nanosphere have been shown below in Figure 3.11 and Figure 3.12 respectively.

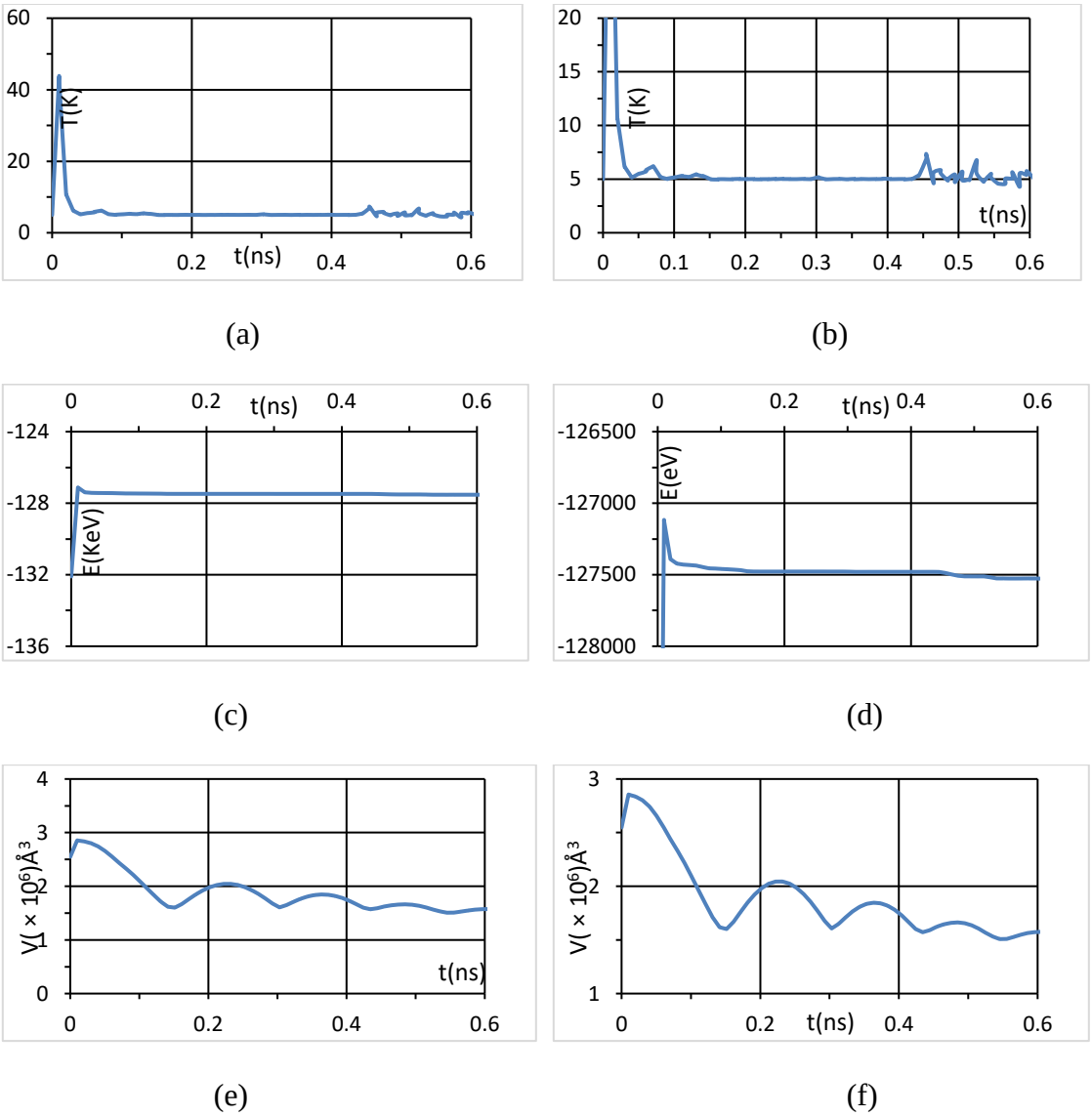

Figure 3.11 Plots of a) Temperature (T) vs Time (t) b) exploded view of T vs t c) Energy (E) vs Time (t) d) exploded view of E vs t e) Volume (V) vs time (t) f) exploded view (V) vs time (t) for the nanosphere with 0 % vacancy and 100 lithium atoms at 5 K.

Before the sample is heated to 300 K, it is important that a complete equilibration at 5 K is achieved so that the nanosphere reaches the state of minimum energy corresponding to its actual physical state at 5 K. As can be seen from Figure 3.11 b, there appears an initial peak in T-t plot at around 0.05 ns. After this the temperature is more or less constant at 5 K till 0.6 ns.

From Figure 3.11 c it can be seen that there is an initial peak in the E-t plot at around 0.05 ns and after this the energy is more or less constant till 0.6 ns and lies close to 127.5 KeV. From 3.11 d, which is a more zoomed plot of E-t, it can be seen that the energy fluctuations are almost absent after 0.05 ns and the final energy is -127,500 electron volts. This suggests that a complete equilibration is achieved at 5 K.

From Figure 3.11 e it can be seen that the initial volume drops from 2.5 million cubic angstroms to close to 1.5 million cubic angstroms in 0.15 ns. From Figure 3.11 f it can be seen that the volume fluctuations beyond 0.2 ns is around 1.5 million cubic angstroms as the sample reaches complete equilibration at 5 K.

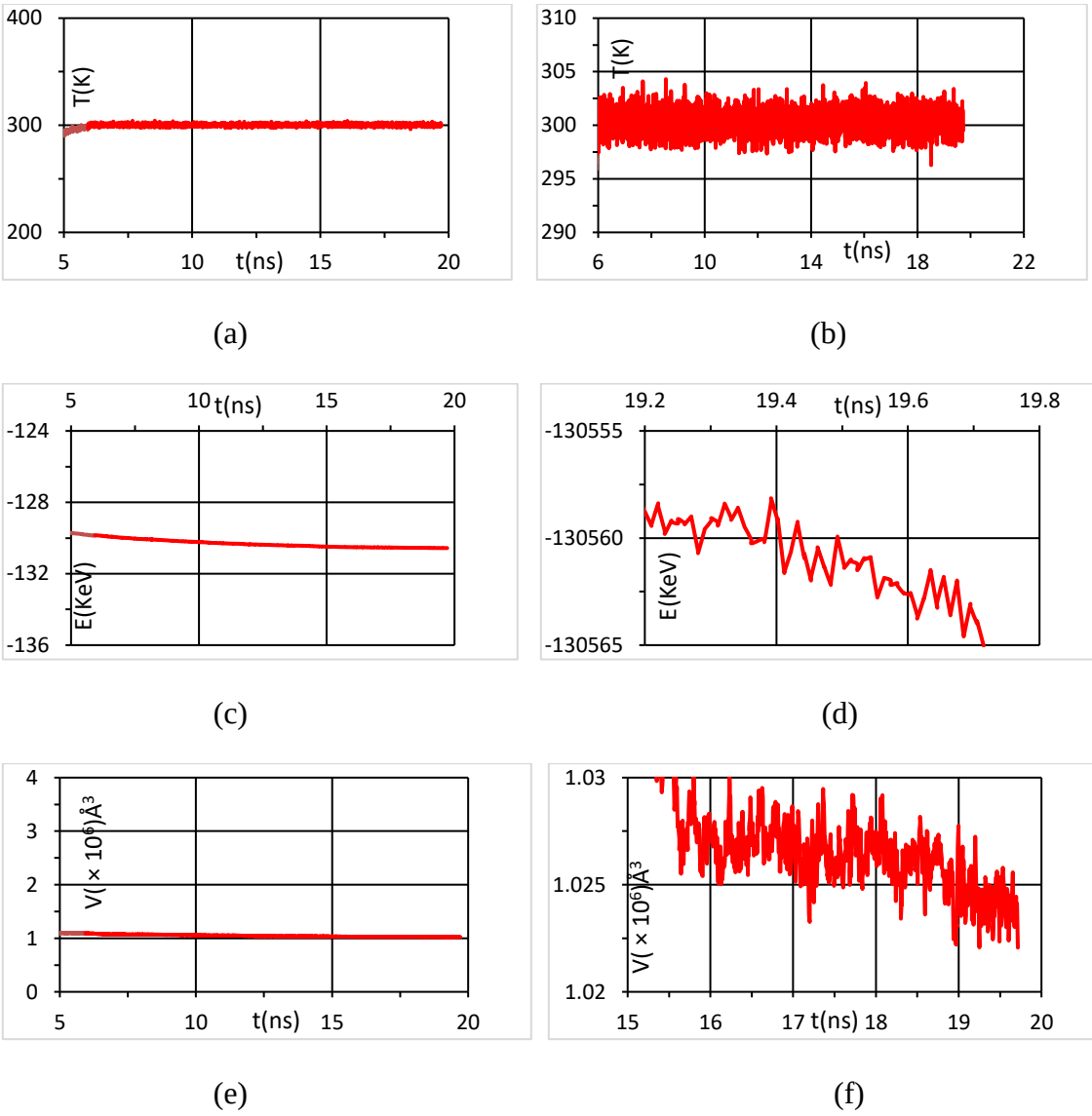

Figure 3.12. Plots of a) Temperature (T) vs Time (t) b) exploded view of T vs t c) Energy (E) vs Time (t) d) exploded view of E vs t e) Volume (V) vs time (t) f) exploded view (V) vs time (t) for the nanosphere with 0 % vacancy and 100 lithium atoms at 300 K.

After the sample is heated to 300 K, it is then equilibrated at 300 K. The time of equilibration is such that there is minimal to no change in the energy. Figure 3.12 a and Figure 3.12 b, show that the temperature of the nanosphere fluctuates around 300 K with the mean value lying at 300 K during the entire course of equilibration step. As can be

seen from Figure 3.12 c, the energy drops from its initial value of -130 KeV to -130.56 KeV after about 19.2 ns. From Figure 3.12 d, it is clear that the mean value of the final energy stays at around -130,560 electron volts between 19.2 to 19.7 ns which confirms that a complete equilibration is achieved at 300 K. Figure 3.12 a and Figure 3.12 b, show that the temperature of the nanosphere fluctuates around 300 K with the mean value lying at 300 K during the entire course of equilibration step. Figure 3.12 e shows that the volume of the sample lies between 1 to 1.5 million cubic angstroms. Figure 3.12 f shows that the volume fluctuations are around the mean volume of about 1.025 million cubic angstroms after 15.5 ns when the sample is completely equilibrated at 300 K.

Having achieved complete equilibration after about 19 ns at 300 K, the diffusion coefficient is now calculated for this sample using the Einstein's formula. The calculated value of the diffusion coefficient is 1.5×10^{-14} m^2/s.

Table 3.1 Diffusion coefficient values obtained with respect to varying vacancy and 100 Li atoms

% fraction vacancy	No. of Li atoms	Diffusion Coefficient, $D(m^2/s) \times 10^{-14}$
0	0	87.7
0	100	1.5
5	100	0.83
20	100	1.17

3.4.5 Diffusion coefficient

Table 3.1 has the values of diffusion coefficient calculated for silicon nanosphere of varying fraction vacancy for 0 Li atom and then a constant number of 100 Li atoms. Notably, these values have been obtained using the MEAM potential. As can be seen from the table that the value of the diffusion coefficient for the case of 0 Li is very much the same as that obtained using the Tersoff potential in Figure 2.12 which was equal to

89×10^{-14} m^2/s. Thus, the values of diffusion coefficients obtained from these two force fields correlates very well. Also, the table shows the values of D obtained for 100 Li atoms for varying fraction vacancy cases.

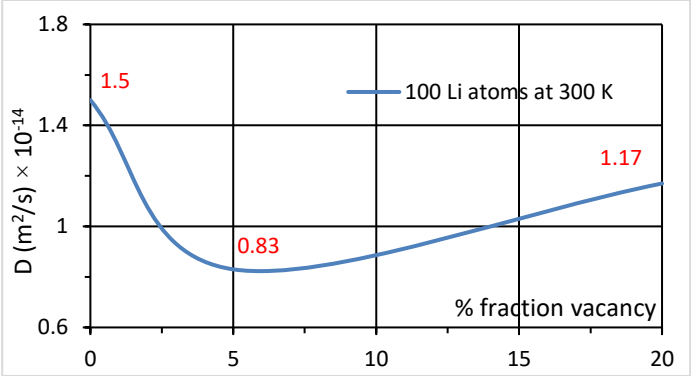

Figure 3.13. Plot of diffusion coefficient, D values vs % fraction vacancy of the nanosphere of radius 5 nm for 100 lithium atoms placed at interstitial sites

As can be seen from Figure 3.13, the behavior of the curve of Li diffusion in silicon nanosphere is non-monotonic in nature. It first decreases to almost half of its value at 0 % fraction vacancy and then increases at 20 % fraction vacancy. The value of D at 20 % fraction vacancy is close to four-fifth of its value at 0 % fraction vacancy. Thus, we can say that the diffusion of dopant atoms is impacted by the presence of fraction vacancy and the extent of this impact is not linear with fraction vacancy. Also, the value of self-diffusion coefficient obtained for silicon is higher than the diffusion coefficient of Li in silicon.

Table 3.2 Diffusion coefficient values obtained with respect to varying vacancy and 0 and100 Li atoms

% fraction vacancy	D_0 (m^2/s) × 10-14	D_{100} (m^2/s) × 10-14	D_0/D_{100}
0	87.7	1.5	58.46
5	82.3	0.83	99.16
20	4530	1.17	3871.8

Table 3.2 shows the value of self-diffusion coefficient of silicon obtained for the nanosphere containing 0 Li atom, D_0; the value of diffusion coefficient for Li diffusion in silicon nanosphere containing 100 Li atoms, D_{100} and their ratio D_0/D_{100}. As can be seen from the table the D_0 increases with increasing fraction vacancy while D_{100} first decreases and then increases with increasing fraction vacancy.

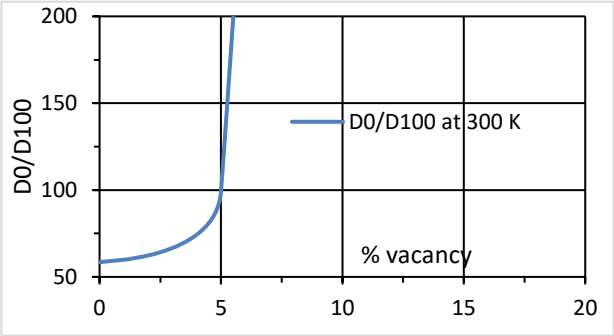

Figure 3.14. Plot of D_0/D_{100} values vs % vacancy of the nanosphere of radius 5 nm for 100 lithium atoms placed at interstitial sites.

From Figure 3.14, it can be seen that the ratio D_0/D_{100} increases by two times of its value at 0 % fraction vacancy while it rises steeply by three orders of magnitude at 20 % fraction

vacancy over its value at 0 % vacancy. It shows that the self-diffusion of silicon is predominantly high at higher fraction vacancy, in this case 20 % fraction vacancy while at lower fraction vacancy, in this case 5 % or below, it is moderately higher than the dopant diffusion.

CHAPTER IV

APPLICATION OF CHARGE EQUILIBRATION TO SMALL NANOCLUSTER

4.1 Charge equilibration

Charge equilibration (QEq), based on the electronegativity equalization principle, a useful method developed for predicting charge distribution in a given system has been successfully applied to polymers, semiconductors, ceramics etc.[40-41] In molecular dynamics studies, charge equilibration yields directly electrostatic energies. In these calculations, charges change as time evolves and so does the electrostatic energy of the material being studied. The input for QEq technique are only the atomic ionization potential (IP), electron affinity (EA) and atomic radius $R_{A.}$ These quantities and the shielded electrostatic interaction are used to create shielded atomic potential. At equilibrium condition, all atomic potentials must be equal which results in equilibrium distribution of charges which are dependent on the geometry.

This technique thus helps overcome the problem of using fixed charges which can respond to changes in local polarization. In the absence of the charge equilibration technique, usually a dielectric constant is included in the force field which can give rise to additional uncertainties in calculations since it is not allowed that the charges change according to local conditions. Charge equilibration method also helps to extend molecular dynamics study to a wide variety of materials such as metals, superconductors, non-standard amino acids and unusual bases and for very useful applications like prediction of infrared intensities and dielectric constants.[42] Under charge equilibration, when the potential energy of the silicon nanocluster changes due to varying electrostatic energy in a molecular dynamics simulation, it is a special point of interest to calculate the self-diffusion coefficient in silicon clusters. This is so because it presents a more realistic environment for prediction of the self-diffusion coefficient in a lithium-ion battery and more accuracy in result. More realistic and accurate prediction of diffusion coefficient

under such conditions is an important mass transport result from the design and operation point of view for the lithium-ion battery.

Energy of an isolated atom, ignoring the higher terms, as a function of charge is given as

$$E_A(Q) = E_{A0} + Q_A \left(\frac{\partial E}{\partial Q}\right)_{A0} + \frac{1}{2} Q_A^2 \left(\frac{\partial^2 E}{\partial Q^2}\right)_{A0} \quad (4.1)$$

$$E_A(+1) = E_{A0} + \left(\frac{\partial E}{\partial Q}\right)_{A0} + \frac{1}{2} \left(\frac{\partial^2 E}{\partial Q^2}\right)_{A0} \quad (4.2)$$

$$E_A(0) = E_{A0} \quad (4.3)$$

$$E_A(-1) = E_{A0} - \left(\frac{\partial E}{\partial Q}\right)_{A0} + \frac{1}{2} \left(\frac{\partial^2 E}{\partial Q^2}\right)_{A0} \quad (4.4)$$

$$\left(\frac{\partial E}{\partial Q}\right)_{A0} = \frac{1}{2} (IP + EA) = \chi_A^0 \quad (4.5)$$

$$\left(\frac{\partial^2 E}{\partial Q^2}\right)_{A0} = IP - EA \quad (4.6)$$

Here IP is the ionization potential and EA is the electron affinity. χ_A is referred as electronegativity,

$$IP - EA = J_{AA}^0 \quad (4.7)$$

Where J_{AA}^0 is Coulombic repulsion for two electrons existing in an orbital and is referred to as the idempotential (self-Coulomb).

Using (4.1), (4.2), (4.3) and (4.4) gives us

$$E_A(Q) = E_{A0} + \chi_A^0 Q_A + \frac{1}{2} J_{AA}^0 Q_A^2 \quad (4.8)$$

In the above equation χ_A^0 and J_{AA}^0 can be derived from atomic data directly and reported in a table in a paper by Rappe and Goddard [J. Phys. Chem. 1991]. The above equation is valid in a restricted sense and is invalid out of the range which may correspond to filling or emptying the valence electronic shells. Proportional to reverse of the size of atom, the Idempotential is given as

$$J_{AA}^{0} = \frac{14.4}{R_{A0}} \tag{4.9}$$

Electrostatic energy $\sum_{A<B} Q_A Q_B J_{AB}$ needs to be evaluated now where J_{AB} is the coulombic interaction between charge centers on A and B.

$$E(Q_1 \ldots . Q_N) = \sum_A \left(E_{A0} + \chi_A^0 Q_A + \frac{1}{2} Q_A^2 J_{AA}^0 \right) + \sum_{A<B} Q_A Q_B J_{AB} \tag{4.10}$$

Which can be re-written as

$$E(Q_1 \ldots . Q_N) = \sum_A (E_{A0} + \chi_A^0 Q_A) + \frac{1}{2} \sum_{A,B} Q_A Q_B J_{AB} \tag{4.11}$$

$$J_{AA}(R) \rightarrow J_{AA}^0 \text{ as } R \rightarrow 0$$

Now we differentiate E with respect to Q_A. This results in an atomic scale potential which is given as

$$\chi_A(Q_1 \ldots . Q_N) = \left(\frac{\partial E}{\partial Q} \right)_A = \chi_A^0 + \sum_B J_{AB} Q_B \tag{4.12}$$

Or,

$$\chi_A(Q_1 \ldots . Q_N) = \chi_A^0 + J_{AA}^0 Q_A + \sum_{B \neq A} J_{AB} Q_B \tag{4.13}$$

where, χ_A is a function of charge on all atoms

For equilibrium, atomic chemical potentials must be all equal which results into N-1 conditions

$$\chi_1 = \chi_2 = \cdots \chi_N \tag{4.14}$$

On providing the condition of total charge, $Q_{tot} = \sum_1^N Q_i$, gives N simultaneous equations. These equations are then solved once for equilibrium self-consistent charges for a structure.

4.2 Proposed work

We apply charge equilibration (QEQ) technique to the MD simulation of a small silicon-lithium nanocluster to obtain the effects of QEQ on the thermodynamics of the silicon-lithium nanocluster and obtain plots of Energy versus time, Temperature versus time,

Coulombic energy versus time and MSD versus time. We also obtain diffusion coefficient, D under conditions of QEQ and compare with case when no QEQ is used at timestep of 1 fs and 10 fs.

4.3 Methodology

Small silicon cluster of sixteen atoms is used such that the total sum of charges is zero and charge on any given atom lie between -0.2 to +0.2 times of an electron charge (e). Molecular dynamics was carried out in metal units with tersoff potential for Si-Si and LJ for Li-Si, Li-Li. Periodic boundary condition, NVT ensemble and a timestep of 1fs was used with was used with $50 \times 50 \times 50$ $Å^3$ simulation box at 300 K. Charge equilibration method applicable for point charges as available in LAMMPS package is used. Alternating steps of the use of charge equilibration fix and molecular dynamics fix in an NVT ensemble is carried out. The resulting charge versus time plots for all the sixteen atoms of the silicon cluster is obtained and compared. Energy versus time, Temperature versus time, Coulombic energy versus time and MSD versus time plots are obtained and compared.

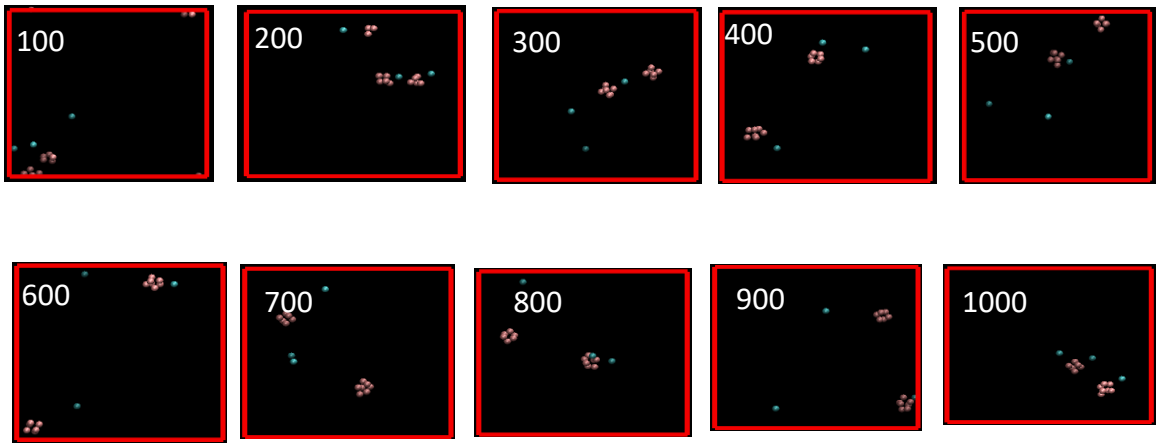

(a)

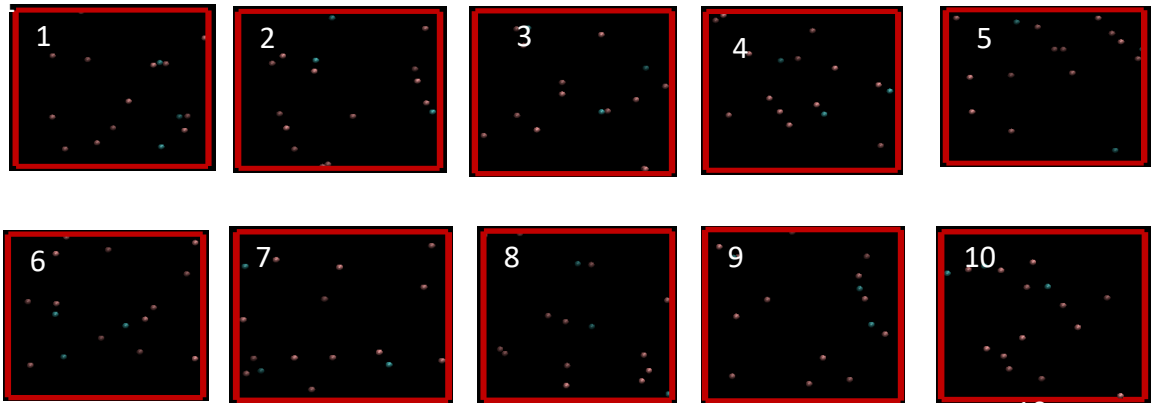

(b)

Figure 4.1. Visualization stages of silicon cluster of 16 atoms containing 13 silicon atoms (red) and 3 lithium atoms (blue) at different times during the simulation with charge equilibration for (a) timestep, dt = 0.001 ps. Number on panels denote time in pico seconds (b) timestep, dt = 0.01 ps. Number on panels denote time in nano seconds.

4.4 Results and discussion

4.4.1 Visualization stages

Figure 4.1 shows the visualization stages of silicon nanocluster of 16 atoms including 3 Lithium atoms at different time of simulation with charge equilibration. As can be seen from Figure 4.1 a, at 300 K, the silicon and lithium atoms are no longer in their respective

lattice positions and move under the combined effects of the force field and charge equilibration. Comparing Figure 4.1 a with Figure 4.1 b, it can be seen that when time step is increased there is greater disorder in this system and the small sub fragmented clusters which are seen in Figure 4.1 a are no longer seen in Figure 4.1 b. Partial charges on silicon and lithium atoms occur as a result of this interaction among the atoms in which both the relative position of each atom charge with respect to time resulting in change of partial charge on it.

4.4.2 Charge versus time plots at timestep of 1 fs

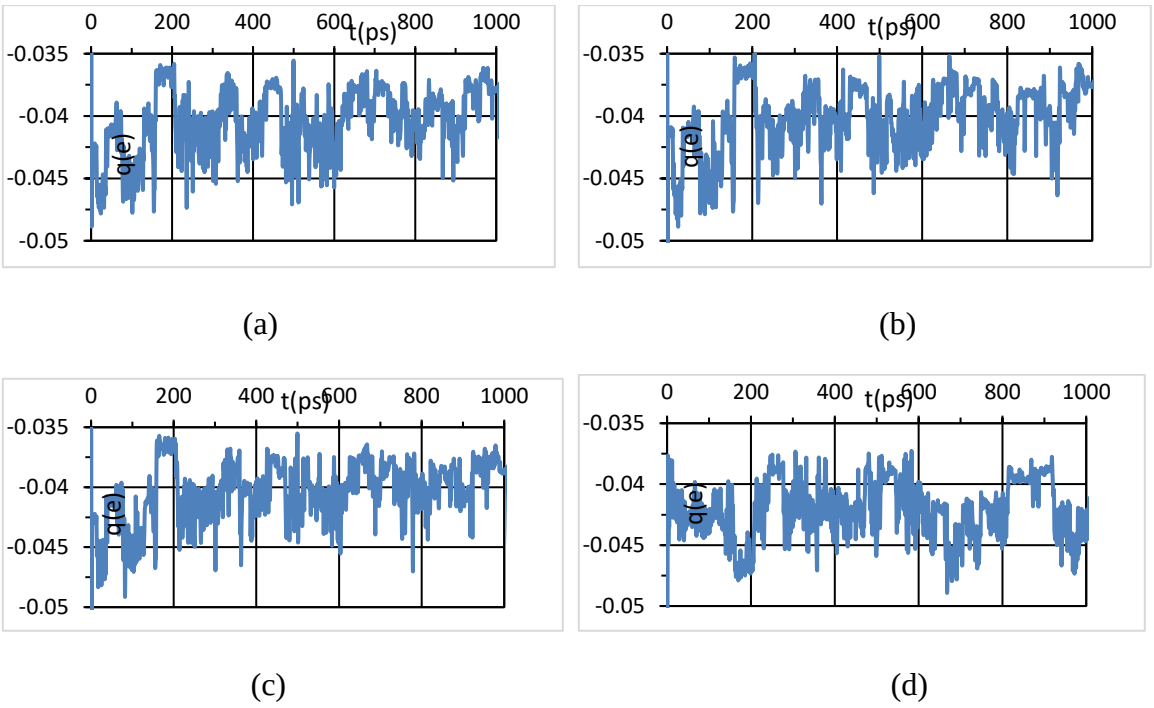

Figure 4.2. Charge, q in terms of an electron charge e, versus time (t) plots for all 16 atoms containing 13 silicon atoms (blue) and 3 lithium atoms (red) for the simulation with charge equilibration for timestep, dt = 0.001 ps.

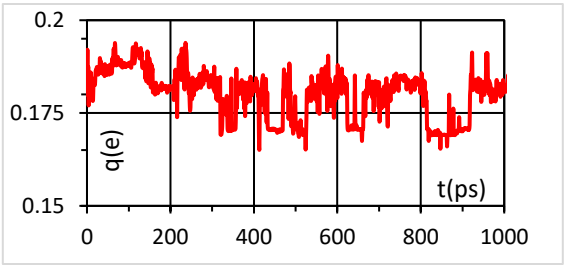

(e)

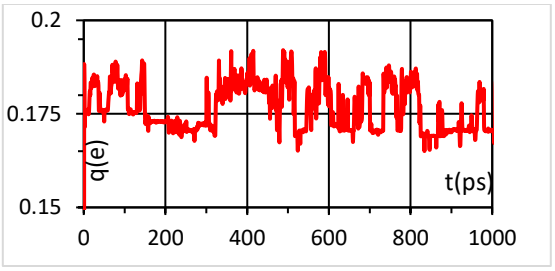

(f)

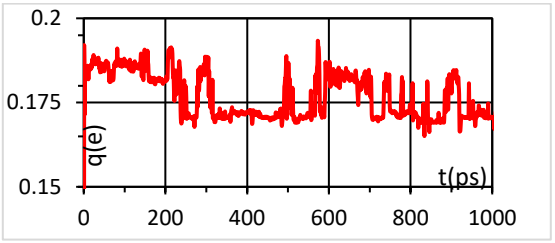

(g)

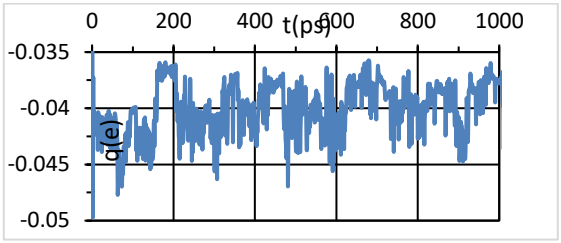

(h)

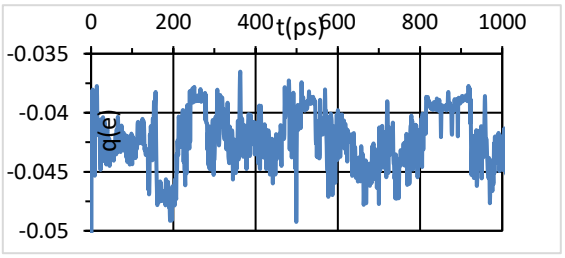

(i)

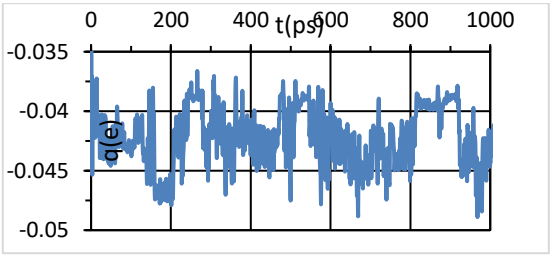

(j)

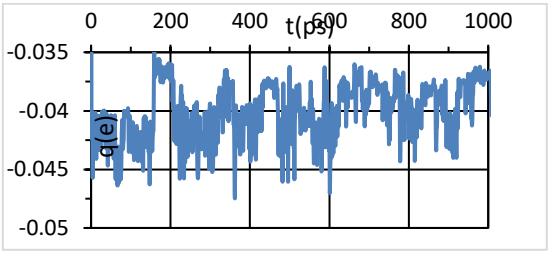

(k)

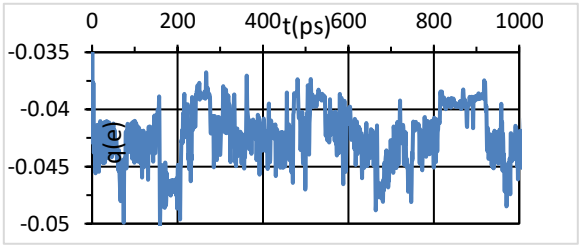

(l)

Figure 4.2 Continued

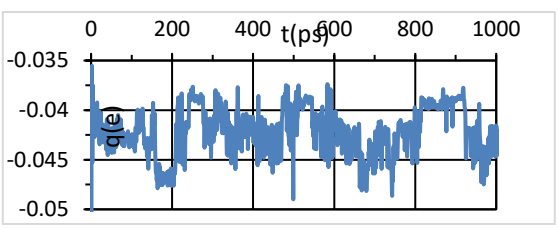

(m)

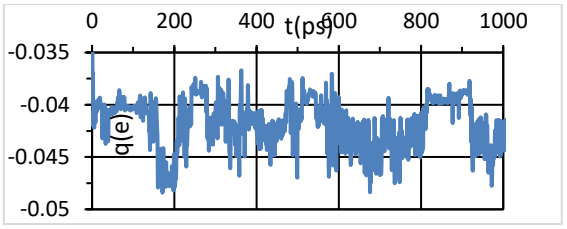

(n)

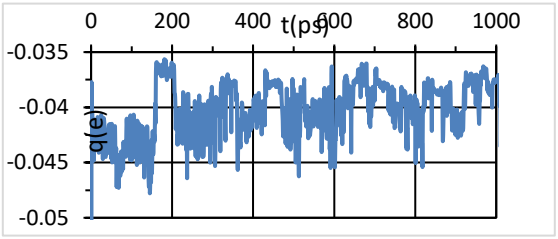

(o)

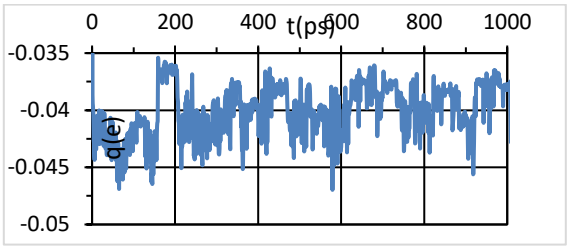

(p)

Figure 4.2 Continued

The variation of charge of each atom with time of simulation has been plotted in Figure 4.2 for time step, t = 0.001 ps. It can be seen that the final charge on silicon atoms are negative and lie between -0.05 to -0.035 while that on the lithium atoms are positive and lie between 0.15 to 0.2. It is to be noted that the final charges appear because of charge equilibration and electronegativity equalization principle. The sum of initial charges is zero and so is the sum of final charges. Silicon is a more electronegative element compared to lithium and hence the partial charges are negative on silicon and positive on lithium.

4.4.3 Charge versus time plots at timestep of 10 fs

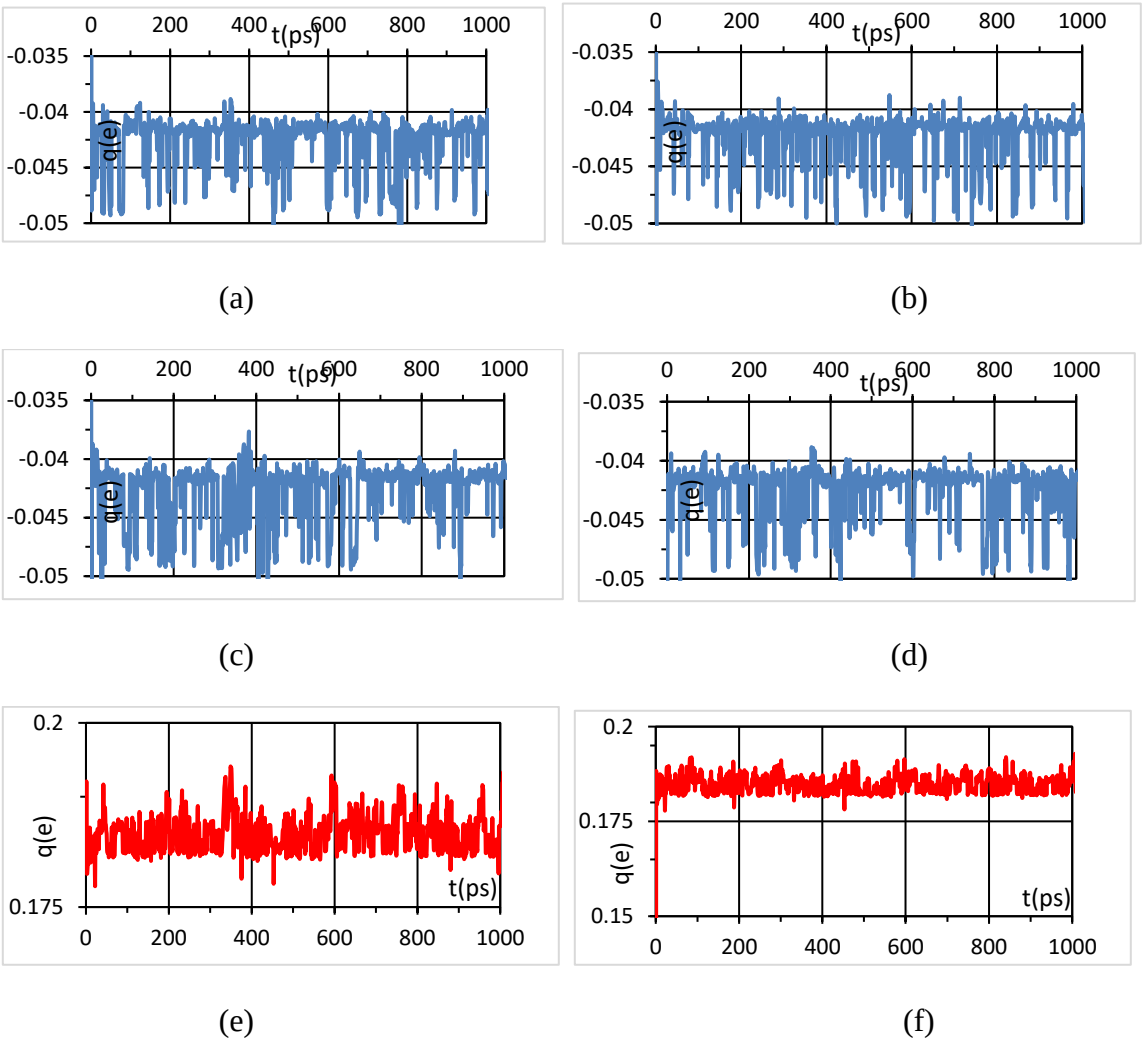

Figure 4.3. Charge, q in terms of an electron charge e, versus time (t) plots for all 16 atoms containing 13 silicon atoms (blue) and 3 lithium atoms (red) for the simulation with charge equilibration for timestep, dt = 0.01 ps.

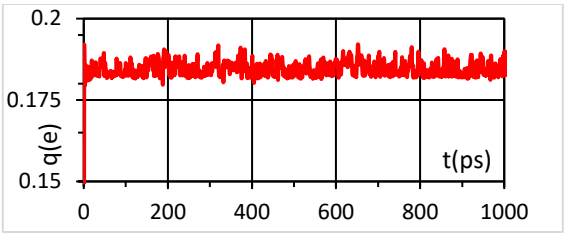

(g)

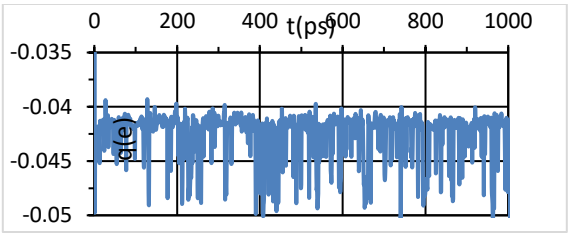

(h)

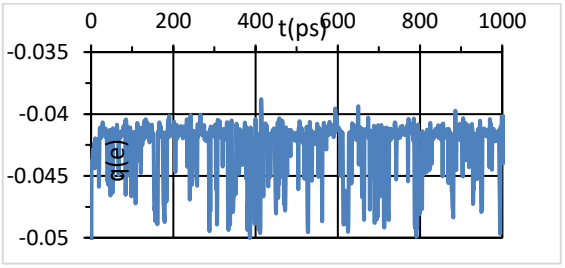

(i)

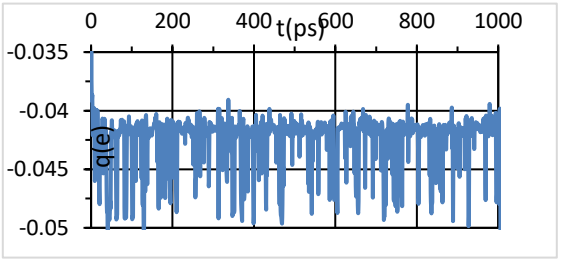

(j)

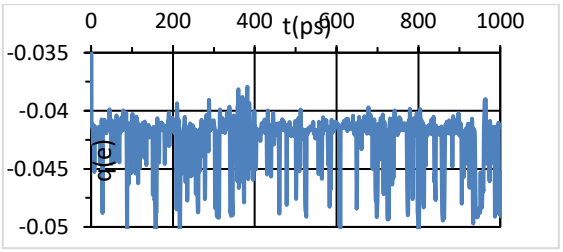

(k)

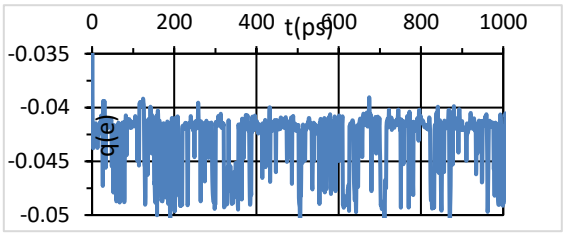

(l)

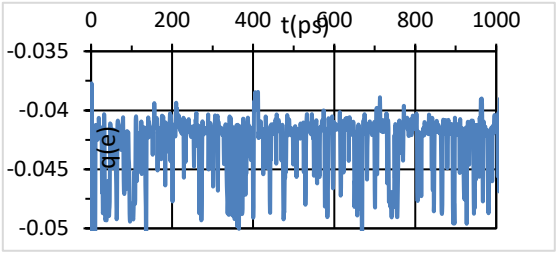

(m)

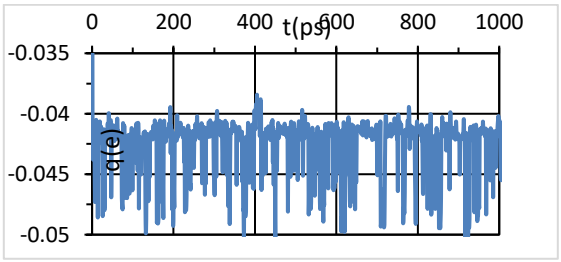

(n)

Figure 4.3 Continued

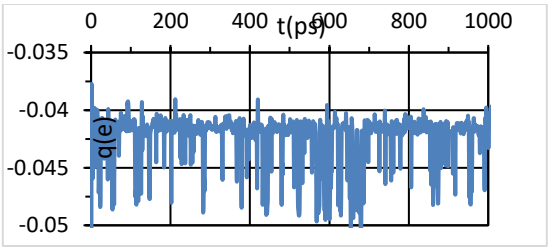

(o)

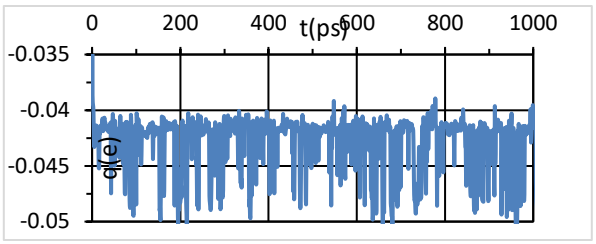

(p)

Figure 4.3 Continued

The variation of charge of each atom with time of simulation has been plotted in Figure 4.3 for time step, t = 0.01 ps. The final charge on silicon atoms are negative and lie between -0.05 to -0.04 while that on the lithium atoms are positive and lie between 0.175 to 0.2. It is to be noted that the final charges appear because of charge equilibration and electronegativity equalization principle. The sum of initial charges is zero and so is the sum of final charges. Silicon is a more electronegative element compared to lithium and hence the partial charges are negative on silicon and positive on lithium.

Table 4.1 Charge on silicon and lithium after first step of charge equilibration

Id	Atom	Initial q(e)
1	Si	-0.049
2	Si	-0.056
3	Si	-0.054
4	Si	-0.050
5	Li	0.192
6	Li	0.188
7	Li	0.192
8	Si	-0.050
9	Si	-0.044
10	Si	-0.037
11	Si	-0.041
13	Si	-0.038
14	Si	-0.040
15	Si	-0.038

Table 4.1 Continued

Id	Atom	Initial q(e)
12	Si	-0.039
16	Si	-0.039

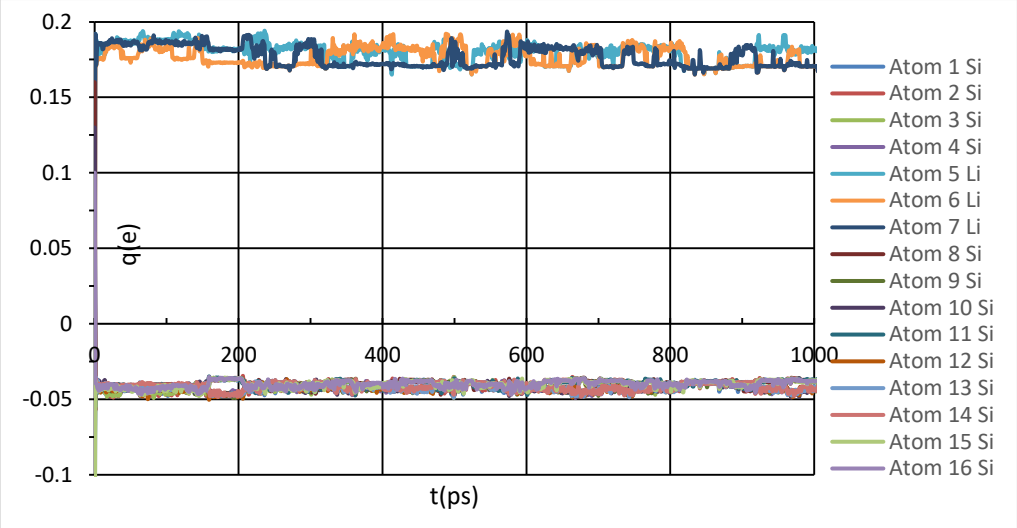

(a)

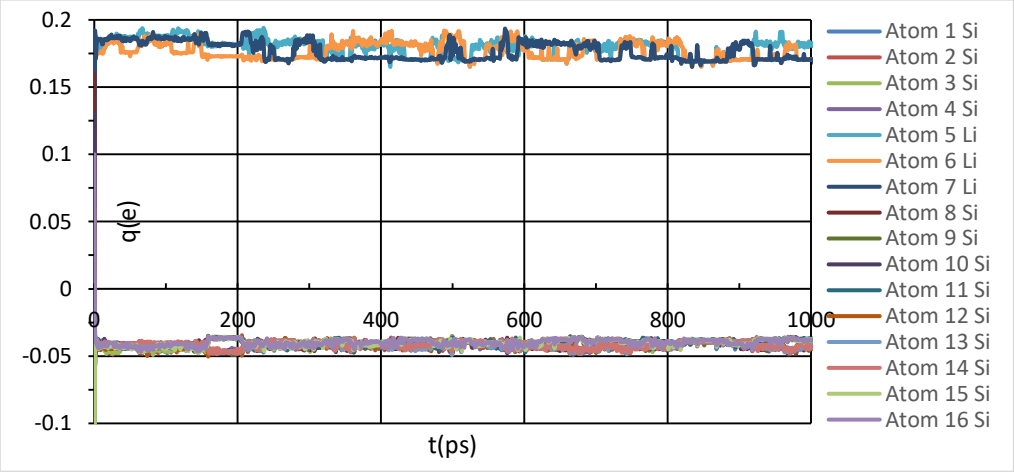

(b)

Figure 4.4. Charge, q in terms of an electron charge e, versus time (t) plots for all 16 atoms containing 13 silicon atoms (blue) and 3 lithium atoms (red) for the simulation with charge equilibration for a) timestep, dt = 0.001 ps b) timestep, dt = 0.01 ps

As can be seen from Figure 4.4 a and b, all the silicon atoms have negative charges and all the lithium atoms have positive charges. On comparing the q versus t plots of Figure 4.4 and Figure 4.4, we see that the range of variation of partial charges in with time step 0.001 ps is more than it is with time step 0.01 ps. This is so because when time step is 0.01 ps for the simulation, there is reduction in time for relative positioning of atoms with respect to each other as compared to when it is 0.001 ps and hence the charges equilibrate accordingly as per the electronegativity equalization.

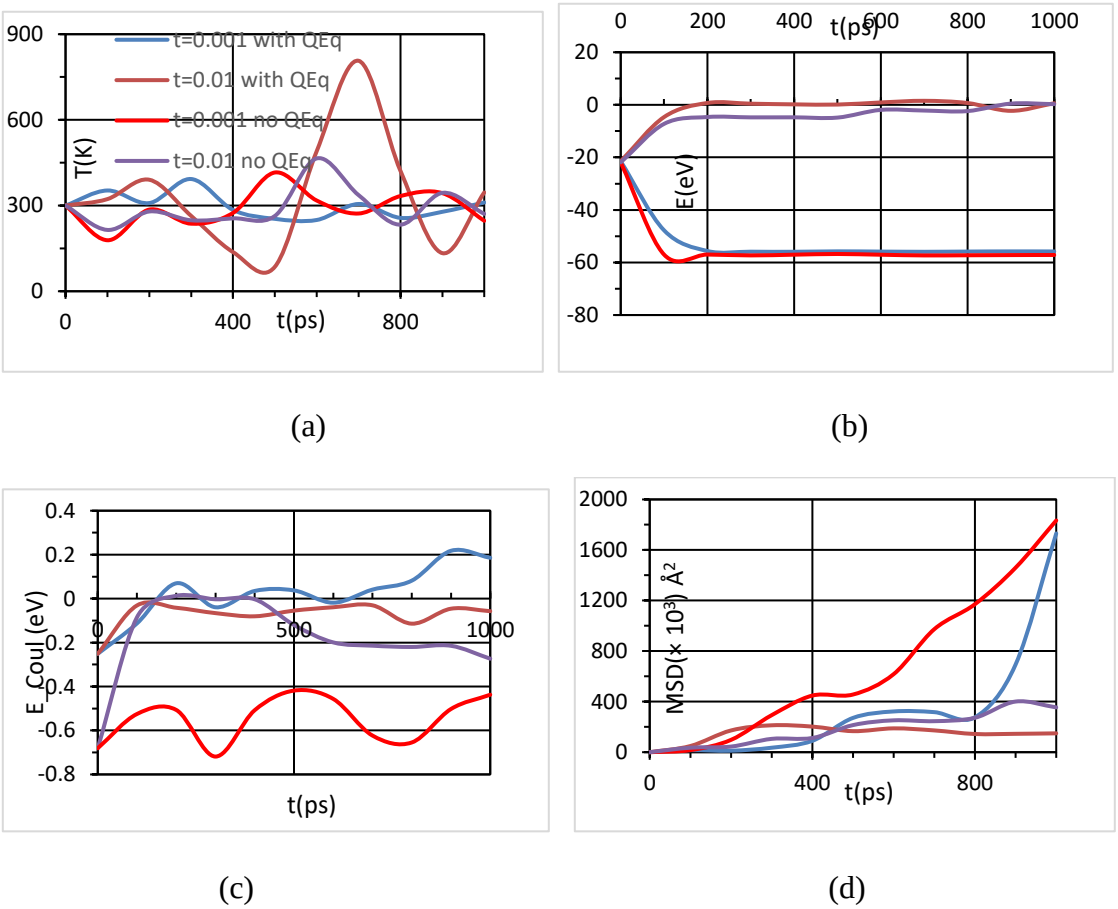

Figure 4.5. Plots of a) Temperature (T) vs time (t) b) Energy (E) vs time (t) c) Coulombic energy (E_Coul) vs time (t) d) mean square displacement, MSD vs time (t) for time step, dt = 0.001 ps and charge equilibration (blue), 0.01 ps and charge equilibration (brown), 0.001 ps and no charge equilibration (red), 0.01 ps and no charge equilibration (purple).

4.4.4 Thermodynamic and transport properties

From Figure 4.5 a it can be seen that the temperature is equilibrated for all the cases and fluctuates around the mean value of 300 K. There is however, a big peak, in T-t plot for the case t = 0.01 ps at around 700 ps. This is indicative that a time step of 0.01 ps may not be optimal and should not be preferred over a time step of 0.001 ps for this simulation as it may take a relatively longer time for the nanocluster to attain equilibration.

From Figure 4.5 b for t = 0.001 ps with charge equilibration and without charge equilibration, there is an initial dip in the E-t plots and the final equilibrated value of energy is around -60 electron volts. However, for t = 0.01 ps with and without charge equilibration, there is an initial rise in the energy and the final equilibrated value is around 0.2 electron volts. This is so because with a smaller value of time step, 0.001 ps in this case, the nanocluster molecular dynamics is more stabilized in terms of energy. Also, for any time step the corresponding plot of energy without charge equilibration is below that of the case with same time step but with charge equilibration. This clearly suggests that when the system is subjected to charge equilibration there is rise in its energy to some extent compared to when it is not. This is so because with charges varying with time during the molecular dynamics, the electrostatic energy is also a significant contributor to the overall energy of the nanocluster.

From Figure 4.5 c it can be seen that for time step, t= 0.001 ps the blue curve which is the case with charge equilibration lies above the red curve which is the case with no charge equilibration. Similarly, for time step, t= 0.01 ps, the brown curve which is the case with charge equilibration lies above the purple curve which is the case with no charge equilibration. Thus, for any time step the corresponding curve of the case with no charge equilibration lies below to that of the case with charge equilibration. This is so because during charge equilibration, the partial charges develop on interacting atoms according to the electronegativity equalization principle.

From Figure 4.5 d it can be seen that for any time step the slope of the MSD vs t curve is lesser for the case with charge equilibration. Also, on comparing the case with time step of 0.001 ps with that of 0.01 ps we find that the slope of the MSD vs t plot is higher for the 0.001 ps case.

Table 4.2 Diffusion coefficient values obtained with respect to varying timesteps and charge equilibration

Simulation type	D(Li) (m^2/s) × 10^{-11}	D(Si) (m^2/s) × 10^{-10}	Ratio of D (Li) (without QEq/with QEq)
t=0.001 ps without QEq	2.98	0.162	2.64
t=0.001 ps with QEq	1.97	0.86	
t=0.01 ps without QEq	0.66	105	4.17
t=0.01 ps with QEq	0.15	86	

Table 4.2 shows the calculated values of diffusion coefficient for the various cases as shown under simulation type. The diffusion coefficient is calculated using the Einstein's formula. As can be seen from the table, clearly the value of diffusion coefficient calculated in conditions of charge equilibration is at least two times smaller for the time step of 0.001 ps and four times smaller for time step 0.01 ps. This suggests at an approach to arriving at a more precise value of diffusion coefficient under practical conditions which may exist in cases where any given nanocluster is subjected to varying charge dynamics as is the case in a lithium-ion battery.

Since charge equilibration takes into account that the charges are distributed as per the electronegativity equalization principle, this effects the way the charges are distributed on each atom unlike when no such condition is placed. Then, the electrostatic interaction between atoms changes which in turn changes the way atoms move during the simulation

and hence their mean square displacement is affected. The strength of the electrostatic interaction decides the impact on the atomic displacement which impacts the mean square displacement. The electronegativity and idempotential values of the atoms are the determining factors for the development of partial charges on atoms which decide the strength of electrostatic interaction.

CHAPTER V

SILICON CAGE ENERGETICS

5.1 Silicon cages

Due to the very high specific capacity (4200 mA h g^{-1}) of silicon compared to graphite (372 mA h g^{-1}), silicon is considered a strong candidate anode material for lithium-ion batteries.[43] However, the major problem in using silicon is the large volume change of the silicon anode during lithiation and delithiation (charge and discharge), resulting in mechanical failure of the anode material. Use of large open surface area silicon nanostructures is a useful prospect. Recently, silicon clathrates have been shown to be a useful material for this purpose.[44,45] A silicon cage is a structure formed with a lithium atom at the center. However, the application of caged structures is currently limited due to knowledge gaps in understanding the lithium transport energetics across the cage.[46]

5.2 Problem statement

Here we want to perform energy calculation and obtain the energy for a complex formed by lithium at the center of a silicon cage. We also propose to study the energetics of a lithium in silicon cage structure using energy minimization which would aid in better understanding of lithiation and delithiation mechanism which is useful in consideration of silicon as anode in lithium ion batteries.

5.3 Methodology

To study the energetics of lithium in silicon cage structure, initially a silicon cage structure will be made using z-matrix such that all silicon atoms in this cage are sp^3 hybridized and the dangling bonds are be satisfied by hydrogen. This cage is then be optimized using the Gaussian optimization software using the RB3PW91 method and 6-31G(d) as the basis set. Once the optimized cage structure is obtained, a lithium atom is introduced at the center of mass of the cage to form the lithium in silicon cage structure. This structure is then further subjected to Gaussian optimization in two different cases, first using a single charge and singlet spin and later using no charge and doublet spin conditions. The energy

difference between these two cases, as calculated from the optimization result is obtained and reported. The resulting optimized structure and the CPU wall times are also observed.

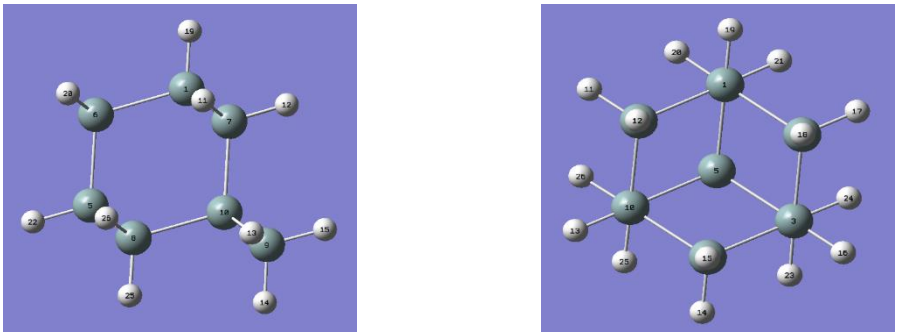

(a) (b)

Figure 5.1. Silicon cage structure geometry optimization using Gaussian.
Calculation Type = FOPT; Calculation Method = RB3PW91, basis set = 6-31G(d)
Images of a) Optimized cage structure from Gaussian output (top view)
b) Optimized cage structure from Gaussian output (side view)

Table 5.1 Z-matrix for the final cage structure

Si1						
Si2	1	2.353608				
Si3	2	2.353604	1	109.7265		
Si4	3	2.353581	2	109.3224	1	59.76269
Si5	4	2.353489	3	109.7672	2	-59.9103
Si6	5	2.353587	4	109.2106	3	59.97636
Si7	1	2.353363	2	109.3596	3	59.8648
Si8	5	2.353487	4	109.3639	3	-59.7463
Si9	3	2.353559	2	109.2926	1	-59.9049
Si10	9	2.353549	3	109.7936	2	59.86282
H11	7	1.493991	1	109.8416	2	179.3886
H12	7	1.494033	1	109.8863	2	61.21511
H13	10	1.496751	9	109.6289	3	-179.992
H14	9	1.493979	3	109.8895	2	-179.205
H15	9	1.493957	3	109.843	2	-61.0228
H16	3	1.496777	2	109.6242	1	179.9605
H17	2	1.493988	1	109.8564	7	-179.195
H18	2	1.493916	1	109.8554	7	-61.0252
H19	1	1.496767	7	109.5926	10	-179.925
H20	6	1.493964	5	109.9073	4	179.1333
H21	6	1.493974	5	109.8514	4	60.92768
H22	5	1.496824	4	109.5847	3	-179.93
H23	4	1.493874	3	109.8649	2	179.1102
H24	4	1.493977	3	109.8257	2	60.94127
H25	8	1.494008	5	109.8239	4	-61.0776
H26	8	1.493924	5	109.8525	4	-179.234

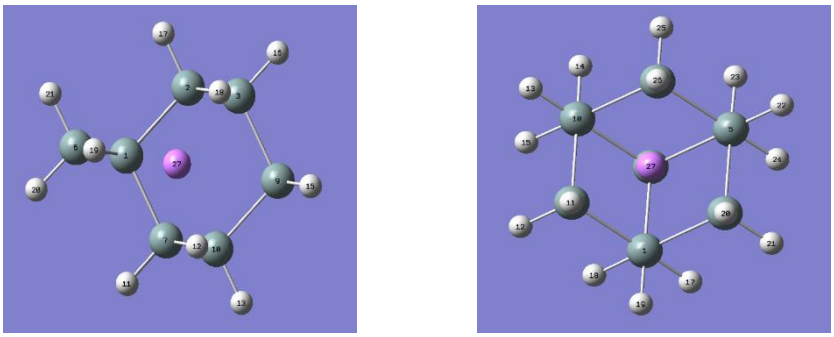

(a) (b)

Figure 5.2. Before optimization complex structure with Li in center. Calculation Type = FOPT; Calculation Method = RB3PW91, basis set = 6-31G(d). Images of a) Optimized cage structure from Gaussian output (top view) b) Optimized cage structure from Gaussian output (side view)

Table 5.2 Z-matrix of the final structure with Li in center and singlet spin

Si1						
Si2	1	2.394604				
Si3	2	2.394361	1	111.9107		
Si4	3	2.394615	2	108.2268	1	58.5539
Si5	4	2.394707	3	111.8567	2	-58.5987
Si6	1	2.394426	2	108.2278	3	-58.5176
Si7	1	2.394359	6	108.2413	5	-58.5318
Si8	5	2.394388	4	108.2678	3	-58.5162
Si9	3	2.394621	2	108.2235	1	-58.5562
Si10	8	2.394451	5	111.8688	4	58.60182
H11	7	1.486721	1	108.4928	6	-61.0798
H12	7	1.486955	1	108.4769	6	178.1241
H13	10	1.486014	8	110.7026	5	179.9722
H14	9	1.4867	3	108.5112	2	178.1489
H15	9	1.486921	3	108.4697	2	-61.0753
H16	3	1.485916	2	110.6269	1	-179.978
H17	2	1.486775	1	108.4666	7	178.2018
H18	2	1.486714	1	108.4486	7	-61.0229
H19	1	1.48593	7	110.7245	10	179.9978
H20	6	1.486747	1	108.5143	7	61.09552
H21	6	1.486814	1	108.4565	7	-178.102
H22	5	1.486091	4	110.666	3	-179.994
H23	4	1.486792	3	108.4761	2	-178.203
H24	4	1.486937	3	108.4946	2	60.97936
H25	8	1.486738	5	108.4848	4	-60.9712
H26	8	1.486757	5	108.4742	4	178.2726
Li27	5	2.429273	4	69.35365	3	0.054338

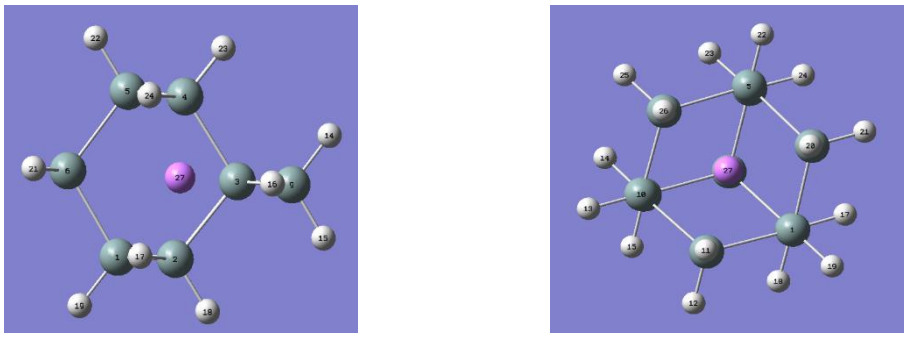

(a) (b)

Figure 5.3. Gaussian optimized complex structure with Li in center and singlet spin. Calculation Type = FOPT; Calculation Method = RB3PW91, basis set = 6-31G(d). Images of a) Optimized cage structure from Gaussian output (top view) b) Optimized cage structure from Gaussian output (side view)

Table 5.3 Z-matrix of the final structure with Li in center and doublet spin

Si1						
Si2	1	2.398133				
Si3	2	2.392857	1	116.2685		
Si4	3	2.384641	2	107.064	1	59.22422
Si5	4	2.384452	3	111.2232	2	-59.4782
Si6	5	2.391947	4	107.2322	3	59.46238
Si7	1	2.472395	6	101.6858	5	-51.3278
Si8	5	2.392155	4	107.2738	3	-59.3853
Si9	3	2.393113	2	110.8378	1	-57.2129
Si10	8	2.397461	5	116.2713	4	58.99111
H11	7	1.493088	1	105.7674	6	-67.8908
H12	7	1.493017	1	106.038	6	176.9839
H13	10	1.523046	8	101.2987	5	-159.157
H14	9	1.493556	3	105.8073	2	-179.529
H15	9	1.49344	3	106.1707	2	-64.9461
H16	3	1.492002	2	110.9229	1	179.1143
H17	2	1.493567	1	110.6595	6	66.05114
H18	2	1.493445	1	109.5188	6	-175.017
H19	1	1.522859	6	101.3498	5	159.2781
H20	6	1.49343	5	106.1073	4	179.0482
H21	6	1.493615	5	105.8826	4	64.40878
H22	5	1.492138	4	109.7134	3	-179.965
H23	4	1.491977	3	109.1754	2	179.8561
H24	4	1.492001	3	109.1796	2	61.16872
H25	8	1.493606	5	105.8553	4	-64.4747
H26	8	1.493464	5	106.071	4	-179.075
Li27	3	2.452609	2	68.57595	1	-1.97828

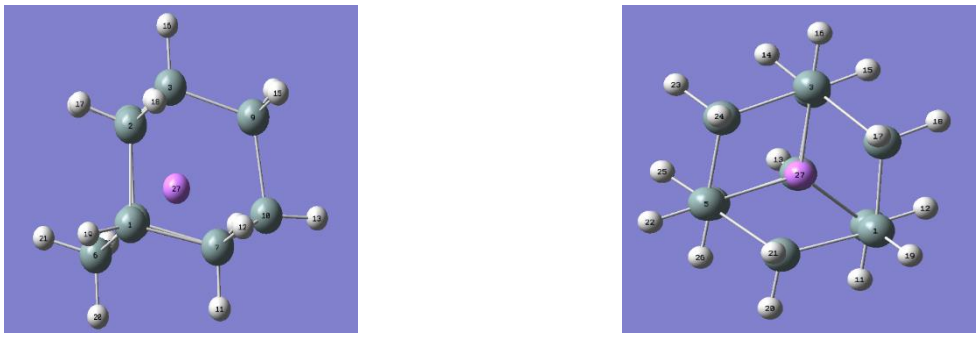

(a) (b)

Figure 5.4. Gaussian optimized complex structure with Li in center and doublet spin. Calculation Type = FOPT; Calculation Method = RB3PW91, basis set = 6-31G(d). Images of a) Optimized cage structure from Gaussian output (top view) b) Optimized cage structure from Gaussian output (side view)

Following is the result of the optimization

Table 5.4 Comparison of optimization results

Parameter	Initial Si cage	Si Cage with Li	Si Cage with Li
Charge	0	1	0
Spin	Singlet	Singlet	Doublet
Energy (eV)	79025.53	79224.36	79228.63
Dipole Moment (Debye)	0.002	0	2.3
CPU Time (min)	70.135	32.518	419.61

Therefore, we find that the difference in the energy of the two-cage structure to be as

= E (cage Li^+) – E (Cage Li) = 4.273 eV

Table 5.5 Charges for the optimized silicon cage structures

ID	Atom	Initial Cage Charge =0, Spin = Singlet	Cage with Li Charge =1, Spin = Singlet	Cage with Li Charge =0, Spin = doublet
1	Si	-0.058737	0.0035130	-0.048703
2	Si	0.130645	0.2261910	0.198052
3	Si	-0.058007	0.0036170	-0.018521
4	Si	0.130257	0.2260370	0.175924
5	Si	-0.058551	0.0033240	-0.018922
6	Si	0.130759	0.2266930	0.195647
7	Si	0.130514	0.2261280	0.230678
8	Si	0.130564	0.2262580	0.196137
9	Si	0.130188	0.2260830	0.19847
10	Si	-0.058052	0.0036700	-0.048957
11	H	-0.037861	0.0043720	-0.035033
12	H	-0.03783	0.0043740	-0.03535
13	H	-0.023926	0.0320870	-0.029326
14	H	-0.037835	0.0043690	-0.034583
15	H	-0.037814	0.0043220	-0.031669
16	H	-0.023953	0.0320830	-0.007923
17	H	-0.037809	0.0043860	-0.034607
18	H	-0.037835	0.0043790	-0.031644
19	H	-0.023917	0.0321100	-0.029274
20	H	-0.037794	0.0043300	-0.031406
21	H	-0.037807	0.0043290	-0.034828
22	H	-0.023929	0.0320650	-0.008121
23	H	-0.037789	0.0043570	-0.030817
24	H	-0.037831	0.0043570	-0.030826
25	H	-0.037846	0.0043700	-0.034815
26	H	-0.037803	0.0043680	-0.03142
27	Li		-0.5521710	-0.588165

CHAPTER VI

CONCLUSIONS

It is found that varying fraction vacancy impacts the thermodynamic and transport properties in silicon nanospheres. Fraction vacancy has a role to play in regulating the heat capacity of nanospheres with fraction vacancy because it is found that for the same input heating conditions different nanospheres having different fraction vacancy heat up with different rates as is indicated by the temperature-time plot. While we find that higher vacancies slow down the rate of heating in general, we also find a certain temperature below which the role of fraction vacancies become more important (200 K here) and above which it is almost insignificant as to what the nanosphere vacancy is in relation to the heating profile of the system. Heating rate of nanospheres do not bear a linear relationship with fraction vacancy. This result could be useful in selecting material with certain fraction vacancy in applications like thermal transducers for temperature below a threshold limit of 200 K. Below the melting point of the silicon clusters and above room temperature, the rate of heating increases as the fraction vacancy increase, but after the melting point, this order reverses. Also, as the boiling point is approached there is again a shift in order of magnitude of the slopes of each fraction vacancy case. This information is useful from the point of view of material selection for a certain heating range based on fraction vacancy consideration. The overall energy of the silicon cluster system with varying vacancies show predictable trend that the nanosphere with the least vacancy has the least overall energy. However, the slopes of energy-time plot indicate that the rate of change of overall energy is impacted by fraction vacancy. With increase in fraction vacancy the nanosphere is in more diffused state at a given temperature and has a relatively higher tendency to reach phase change early compared to the case with lesser fraction vacancy. Thus, fraction vacancy of a nanosphere impacts its structural integrity since a nanosphere with higher fraction vacancy tends to disintegrate faster compared to the nanosphere having lesser fraction vacancy.

At 300 K, the self-diffusion coefficient, D values vary non-monotonically i.e. the D value increases as we go to 2.5 % vacancy from 0 % vacancy, then decreases at 5 % and is the least at 7.5 % before increasing steeply at 10 % and 20 % fraction vacancy. The striking result is that beyond a certain threshold fraction vacancy, there is close to two order magnitude of increase in the self-diffusion coefficient. However, the D value monotonically increases, even though marginally, for these fraction vacancies at 2000 K suggesting that at temperatures beyond melting point of silicon, the effect of fraction vacancy on regulating self-diffusion is contrasting and less compared to that at room temperature.

The value of the diffusion coefficient obtained using MEAM potential for the case of 0 Li and 0 % fraction vacancy is very much the same as that obtained using the Tersoff potential for silicon nanospheres. Thus, the values of diffusion coefficients of Si in Si obtained from these two force fields correlates very well. It is found that as fraction vacancy increases, the diffusion coefficient value of Li displays non-monotonic behavior for the same number of Li atoms. It first decreases to almost half of its value at 0 % fraction vacancy and then increases at 20 % fraction vacancy. The value of D at 20 % fraction vacancy is close to four-fifth of its value at 0 % fraction vacancy. Thus, we can say that the diffusion of dopant atoms too is impacted by the presence of fraction vacancy and the extent of this impact is not necessarily linear with fraction vacancy. .

When charge equilibration technique was applied to a small silicon nanocluster containing 13 silicon atoms and 3 lithium atoms having initial some initial charges, it was found that the final partial developed differently on different atoms as per the electronegativity equalization principle such that the final sum of charges was zero. Irrespective of the sign of initial charges on lithium and silicon, the final charges had all positive sign for lithium and negative sign for silicon atoms. Charge dynamics was relatively more stable at 1 fs as compared to that at 10 fs timestep of simulation. Charge equilibration impacted the thermodynamic and transport property of the silicon-lithium nanocluster as could be

concluded from temperature versus time, energy versus time, MSD versus time plots and the diffusion coefficient values. Charge equilibration elevated the energy and coulombic energy of the silicon-lithium nanocluster as compared to when no charge equilibration was employed. However, charge equilibration reduced the value of diffusion coefficient as compared to when no charge equilibration was employed. The reduction effect was more pronounced for the 10 fs timestep than 1 fs timestep. Thus, charge equilibration suggests at an approach for arriving at a more precise value of diffusion coefficient under practical conditions which may exist in cases where any given nanocluster is subjected to varying charge dynamics as is the case in a lithium-ion battery.

We found that the difference in the energy of the silicon cage structure with positively charged lithium atom at its center of mass and the silicon cage structure with neutral lithium at the center of the mass of the cage to be 4.273 eV. This value points at the ionization energy of the structure.

REFERENCES

1. Andersen, H. C., Molecular dynamics simulations at constant pressure and/or temperature. *The Journal of Chemical Physics* **1980,** *72* (4), 2384-2393.

2. Robinson, J. E., On quantum extensions of classical molecular dynamics. *Bulletin of the American Physical Society* **1978,** *23* (3), 250-250.

3. Rode, B. M., Classical versus quantum mechanical simulations: The accuracy of computer experiments in solution chemistry. *Novel Approaches to the Structure and Dynamics of Liquids: Experiments, Theories and Simulations*. **2004**, 41-52.

4. Cui, Z.; Gao, F.; Cui, Z.; Qu, J., A second nearest-neighbor embedded atom method interatomic potential for Li–Si alloys. *Journal of Power Sources* **2012,** *207* (Supplement C), 150-159.

5. Baskes, M. I.; Johnson, R. A., Modified embedded atom potentials for HCP metals. *Modelling and simulation in materials science and engineering* **1994,** *2* (1), 147-163.

6. Dodson, B., Development of a many-body Tersoff-type potential for silicon. *Physical review. B, Condensed matter* **1987,** *35* (6), 2795-2798.

7. Srivastava, D.; Garrison, B.; Brenner, D., Modeling the growth of semiconductor epitaxial films via nanosecond time scale molecular dynamics simulations. *Langmuir* **1991,** *7* (4), 683-692.

8. Wang, J.; Rockett, A., Simulating diffusion on Si(001) 2×1 surfaces using a modified interatomic potential. *Physical review. B, Condensed matter* **1991,** *43* (15), 12571-12579.

9. Balamane, H.; Halicioglu, T.; Tiller, W. A., Comparative study of silicon empirical interatomic potentials. *Physical review. B, Condensed matter* **1992,** *46* (4), 2250-2279.

10. Plimpton, S., Fast parallel algorithms for short-range molecular dynamics. *Journal of computational physics* **1995,** *117* (1), 1-19.

11. Plimpton, S., A new parallel method for molecular dynamics simulation of macromolecular systems. *Journal of computational chemistry* **1996,** *17* (3), 326-337.

12. Brown, W. M.; Wang, P.; Plimpton, S.; Tharrington, A., Implementing molecular dynamics on hybrid high performance computers – short range forces. *Computer physics communications* **2011,** *182* (4), 898-911.

13. Brown, W. M.; Kohlmeyer, A.; Plimpton, S.; Tharrington, A., Implementing molecular dynamics on hybrid high performance computers – Particle–particle particle-mesh. *Computer physics communications* **2012,** *183* (3), 449-459.

14. Humphrey, W.; Dalke, A.; Schulten, K., VMD: Visual molecular dynamics. *Journal of molecular graphics* **1996,** *14* (1), 33-38.

15. Ho, K.-M.; Shvartsburg, A. A.; Pan, B.; Lu, Z.-Y.; Wang, C.-Z.; Wacker, J. G.; Fye, J. L.; Jarrold, M. F., Structures of medium-sized silicon clusters. *Nature* **1998,** *392* (6676), 582-585.

16. Pacchioni, G.; Koutecký, J., Silicon and germanium clusters. A theoretical study of their electronic structures and properties. *The Journal of Chemical Physics* **1986,** *84* (6), 3301-3310.

17. Raghavachari, K., Theoretical study of small silicon clusters: Cyclic ground state structure of Si_3. *The Journal of Chemical Physics* **1985,** *83* (7), 3520-3525.

18. Wong, H., Recent developments in silicon optoelectronic devices. *Microelectronics Reliability* **2002,** *42* (3), 317-326.

19. Gu, M.; He, Y.; Zheng, J.; Wang, C., Nanoscale silicon as anode for Li-ion batteries: The fundamentals, promises, and challenges. *Nano Energy* **2015**, Medium: X; Size: p. 366-383.

20. Lee, S. W.; McDowell, M. T.; Berla, L. A.; Nix, W. D.; Cui, Y., Fracture of crystalline silicon nanopillars during electrochemical lithium insertion. *Proceedings of the National Academy of Sciences of the United States of America* **2012,** *109* (11), 4080-4085.

21. Fairfield, J. M.; Masters, B. J., Self-diffusion in intrinsic and extrinsic silicon. *Journal of Applied Physics* **1967,** *38* (8), 3148-3154.

22. Konstantinov, A. O., Injection of nonequilibrium point-defects during diffusion of impurities in crystals with a mixed self-diffusion mechanism. *Soviet physics. Semiconductors* **1991,** *25* (7), 710-714.

23. Blochl, P. E., First principles calculations of self-diffusion coefficients in silicon physics of semiconductors - proceedings of the 20th international conference (in 3 volumes). **1990**, 533-536.

24. Kube, R.; Bracht, H.; Hüger, E.; Schmidt, H.; Hansen, J. L.; Larsen, A. N.; Ager, J. W.; Haller, E. E.; Geue, T.; Stahn, J., Contributions of vacancies and self-interstitials to self-diffusion in silicon under thermal equilibrium and nonequilibrium conditions. *Physical Review B* **2013,** *88* (8), 085206.

25. Coquil, T.; Fang, J.; Pilon, L., Molecular dynamics study of the thermal conductivity of amorphous nanoporous silica. *International Journal of Heat and Mass Transfer* **2011,** *54* (21), 4540-4548.

26. Huang, P.-H.; Lu, C.-M., Effects of vacancy cluster defects on electrical and thermodynamic properties of silicon crystals. *The Scientific World Journal* **2014,** *2014*, 8.

27. Ural, A.; Griffin, P. B.; Plummer, J. D., Self-diffusion in silicon: Similarity between the properties of native point defects. *Physical Review Letters* **1999,** *83* (17), 3454-3457.

28. Zhao, K.; Pharr, M.; Vlassak, J. J.; Suo, Z., Inelastic hosts as electrodes for high-capacity lithium-ion batteries. *Journal of Applied Physics* **2011,** *109* (1), 016110.

29. Wang, H.; Ji, X.; Chen, C.; Xu, K.; Miao, L., Lithium diffusion in silicon and induced structure disorder: A molecular dynamics study. *AIP Advances* **2013,** *3* (11), 112102.

30. Leuken, H. v.; de Wijs, G. A.; van der Lugt, W.; Groot, R. A. d., Electronic structure of $Li_{12}Si_7$. *Physical Review B* **1996,** *53* (16), 10599-10604.

31. Chevrier, V. L.; Zwanziger, J. W.; Dahn, J. R., First principles study of Li–Si crystalline phases: Charge transfer, electronic structure, and lattice vibrations. *Journal of Alloys and Compounds* **2010,** *496* (1), 25-36.

32. Tritsaris, G. A.; Zhao, K.; Okeke, O. U.; Kaxiras, E., Diffusion of lithium in bulk amorphous silicon: A theoretical study. *The Journal of Physical Chemistry C* **2012,** *116* (42), 22212-22216.

33. Yan, X.; Gouissem, A.; Sharma, P., Atomistic insights into Li-ion diffusion in amorphous silicon. *Mechanics of Materials* **2015,** *91* (Part 2), 306-312.

34. Fedorov, A. S.; Popov, Z. I.; Kuzubov, A. A.; Ovchinnikov, S. G., Theoretical study of the diffusion of lithium in crystalline and amorphous silicon. *Journal of Experimental and Theoretical Physics Letters* **2012,** *95* (3), 143-147.

35. Peng, B.; Cheng, F.; Tao, Z.; Chen, J., Lithium transport at silicon thin film: Barrier for high-rate capability anode. *The Journal of Chemical Physics* **2010,** *133* (3), 034701.

36. Haldar, P.; Chatterjee, A., Nudged-elastic band study of lithium diffusion in bulk silicon in the presence of strain. *Energy Procedia* **2014,** *54* (Supplement C), 310-319.

37. Lee, H.-S.; Lee, B.-J., Structural changes during lithiation and delithiation of Si anodes in Li-ion batteries: A large scale molecular dynamics study. *Metals and Materials International* **2014,** *20* (6), 1003-1009.

38. Groh, S.; Alam, M., Fracture behavior of lithium single crystal in the framework of (semi-)empirical force field derived from first-principles. *Modelling and simulation in materials science and engineering* **2015,** *23* (4), 045008.

39. Wang, H.; Chew, H., Molecular dynamics simulations of plasticity and cracking in lithiated silicon electrodes. *Extreme Mechanics Letters* **2016,** *9* (3_supplement), 503-513.

40. Rappe, A. K.; Goddard, W. A., Charge equilibration for molecular dynamics simulations. *The Journal of Physical Chemistry* **1991,** *95* (8), 3358-3363.

41. Wilmer, C. E.; Kim, K. C.; Snurr, R. Q., An extended charge equilibration method. *The Journal of Physical Chemistry Letters* **2012,** *3* (17), 2506-2511.

42. Lucas, T. R.; Bauer, B. A.; Patel, S., Charge equilibration force fields for molecular dynamics simulations of lipids, bilayers, and integral membrane protein systems. *Biochimica et biophysica acta* **2012,** *1818* (2), 318-329.

43. Ozanam, F.; Rosso, M., Silicon as anode material for Li-ion batteries. *Materials Science and Engineering: B* **2016,** *213*, 2-11.

44. Warrier, P.; Koh, C. A., Silicon clathrates for lithium ion batteries: A perspective. *Applied Physics Reviews* **2016,** *3* (4), 040805.

45. Li, Y.; Chan, C. K., Ternary type I silicon clathrates for lithium-ion battery anodes. *Meeting Abstracts* **2015,** *MA2015-02* (6), 498.

46. Zhao, K.; Wang, W. L.; Gregoire, J.; Pharr, M.; Suo, Z.; Vlassak, J. J.; Kaxiras, E., Lithium-assisted plastic deformation of silicon electrodes in lithium-ion batteries: A first-principles theoretical study. *Nano Letters* **2011,** *11* (7), 2962-2967.